# Fluctuating pressures in high-enthalpy geothermal wells in the Hengill area in Iceland

## An investigation based on simulations of two-phase flow instabilities

by


| Student Name | Student Number |
|---|---|
| Tessa Hornes | 5379970 |
| Rafaël Cox | 5572045 |
| Ethan Meen | 5583063 |
| Michael Knott | 6217680 |
| Linda Kuusik | 5467373 |



Course: CEGM3000

Faculty: Faculty of Civil Engineering and Geosciences, Delft

Supervisors: Prof. Dr. S. (Sebastian) Geiger, T. (Tobias) Schmiedel, S. (Sigurður) Ragnarsson


TU Delft Reykjavík Energy

# Contents

# List of Figures

# Abstract

This report aims to find the underlying cause of pressure fluctuations in five Icelandic geothermal wells. These fluctuations affect the productivity of the power plant; making it relevant to understand their causes and mitigation measures. Based on the available data we concluded that the fluctuations do not originate in the reservoir or surface infrastructure but in the well bore. We then proceeded to follow two hypotheses to explain fluctuations within the well bore.

The first one, we called Internal Flow Instability. It describes oscillating behaviour as a result of Ledinegg instability, where small instabilities in momentum balance become amplified along the well. To further explore this theory we built a 1D numerical model for two-phase flow. We plotted the characteristic curve (i.e. the relation between pressure drop and flow rate) for an example stable and unstable well. Our results show that the operating condition of the stable well lies in the stable region of the curve, and vice versa. The curves do predict the stability of the wells, correctly but do not give an explanation for the instability.

The second hypothesis examined in this report is the Multiple Feed Zones theory. This hypothesis investigates how different feed zones supplying fluids of different enthalpies mix within a well bore; focusing on the interactions between two phase flow in the well bore and single phase flow from the feed zones. A STARS model was developed to test whether single-phase flow could exist above a two-phase region in the well bore, and the simulations confirmed that this is feasible. To further investigate the mechanism, we applied the model from Matsumoto et al. (2020). This model was used as a proof of concept to demonstrate that interactions between multiple feed zones with different enthalpies can produce the type of fluctuations observed in the wells. While the simulated fluctuations do not match the observed frequency, the results support that, under the modelled conditions, the Multiple Feed Zones theory could provide an explanation for the pressure oscillations observed in the wells.

# 1 Introduction

For a geothermal plant to generate electricity and heat consistently, it requires a constant supply of water and steam. Instabilities in production wells, however, can cause pressure and flow rates to fluctuate. These fluctuations affect the plant's overall productivity and must be minimized. Ensuring the plants performance, therefore, depends on identifying the root causes of this instability to mitigate their impact on the system.

For this project, five geothermal production wells from Reykjavík Energy have been studied. Through their geothermal plants and hydropower plants, Reykjavík Energy supplies 70% of Icelandic households with district heating and 60% of households with electricity [34]. Currently, 66% of total primary energy in Iceland comes from geothermal [10], making it the main energy source for Icelanders. This highlights the importance of making geothermal energy supply as reliable and predictable as possible through stabilising the flow in the wells. However, these five wells are found to have fluctuating pressure outputs whereas the majority of wells producing in the same area, from the same formations around the Hengill volcano, operate at near constant pressure and flow rate. The geothermal production wells considered in this project are located around the Hengill volcano in Iceland, where two high enthalpy geothermal fields are located on either sides of the central volcano as shown in Figure 1.1.

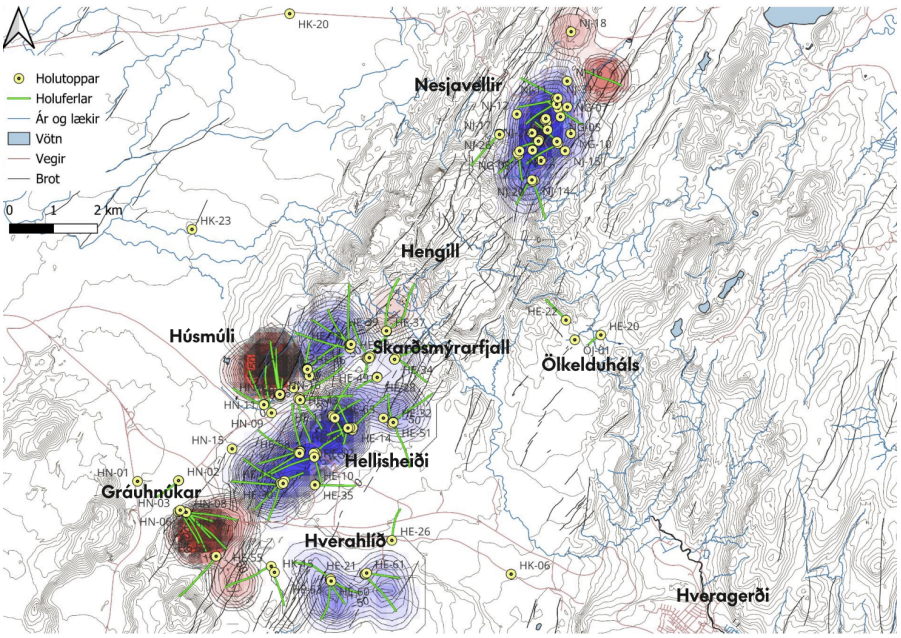


**Figure 1.1:** Hengill geothermal area.[35]

The main objective of this report is to find out the cause of fluctuating wellhead pressures and test our hypotheses by modelling two phase flow in a well bore using different approaches with different assumptions. Furthermore, sensitivity analysis is conducted to discover which parameters contribute the most to the disruptions in the flow. Additionally, solutions are provided from the literature that could potentially limit the fluctuating behaviour, but these could not be reliably confirmed by our

models.

The report is structured in the following way: in Chapter 2 the background information of the project is given including geology; well locations and geometry; data provided by Reykjavík Energy. Some of the data has been visualised for easier understanding. In Chapter 3 the problem is explained further and accompanied with possible hypotheses that cause the fluctuating phenomena. Half of the theories will be disregarded in this chapter and the two most promising ones will be described in detail in Chapters 4 and 5. In these chapters, the underlying physics of each hypothesis will be explained further, followed by an explanation of modelling approaches, results, sensitivity analysis and discussion about limitations. After both theories have been described separately, discussion in Chapter 6 compares them and summarises the pros and cons of each of them. Conclusions can be found under Chapter 7.

# 2 Project description

The objective of this project is to find an explanation for the pressure fluctuations found in five high-enthalpy geothermal production wells around the Hengill volcano in Iceland. This chapter will introduce the problem statement (Section 2.1), the geology of the area (Section 2.2) and then describes the five wells studied in this report (Section 2.3). Section 2.4 gives an overview of the available data and Section 2.5 illustrates the pressure fluctuations of each well.

## 2.1. Problem statement

The geothermal fields of Hellisheiði and Nesjavellir contain 72 production wells, of which only five show cyclical wellhead pressure fluctuations, the others do not show such oscillations and operate normally. As shown in figure 2.2 the fluctuating wells are not isolated or grouped, but spread throughout the whole geothermal area. As pressure fluctuations can disrupt the energy production of the geothermal system, they should be understood and minimized. This report aims to answer the following question: "What is causing the pressure fluctuations?". Therefore, all three components of the system — including the reservoir, well bore, and surface infrastructure — should be taken into account when assessing the overall influence on the pressure fluctuations.

## 2.2. Geology

To take a first investigative look at the reservoir, the overall geology of the area was considered.High enthalpy geothermal systems are defined as having an average fluid enthalpy of 1300 kJ/kg to 2500 kJ/kg with temperatures generally between 250 °C - 330 °C [32]. The geothermal wells in the two fields around the Hengill volcano have an average fluid enthalpy of 1580 kJ/kg in Hellisheiði and 1570 kJ/kg in Nesjavellir, classifying them as high-enthalpy wells [35]. High-enthalpy wells produce water and steam hot enough to directly produce electricity. In this particular area the high heat flow required for the high-enthalpy geothermal fluid comes from shallow level crustal magma chambers or dyke swarms [37].

Iceland is situated on the Mid-Atlantic Ridge, a divergent plate boundary and on top of a mantle plume. The island started forming 24 million years ago [15]. The Mid-Atlantic Ridge is represented on Iceland as the Kolbeinsey Ridge (KR) in the north and the Reykjanes Ridge (RR) in the south as illustrated on the left of Figure 2.1. On land, the Ridge characterized by Northern Volcanic Zone (NVZ) and the Western Volcanic Zone (WVZ) which are offset in the region known as the Mid-Icelandic Volcanic Zone (MVZ), a transform fault [15] . The Northern Volcanic Zone is connected to the Kolbeinsey Ridge and the Eastern Volcanic Zone (EVZ) whereas the Western Volcanic Zone is connected to the Reykjanes Ridge. The Western and Eastern Volcanic Zones are connected through the South Icelandic Seismic Zone (SISZ), as illustrated on the right of Figure 2.1.

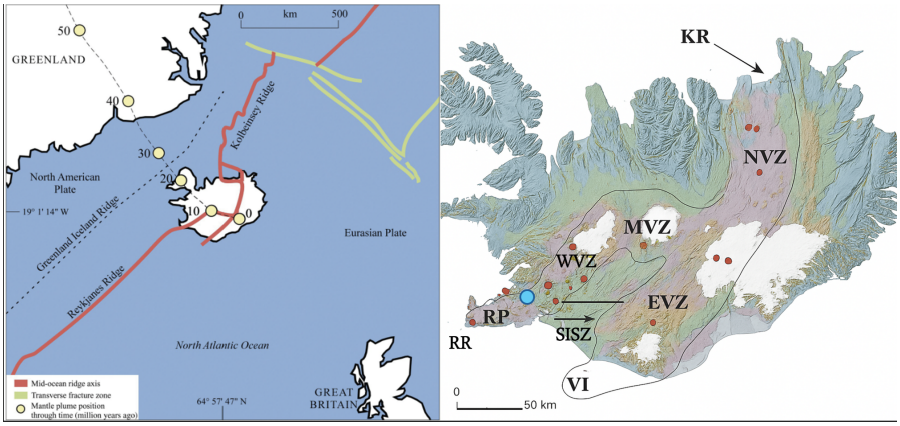


**Figure 2.1:** Left: location of ridges and mantle plume. Right: location of volcanic zones and the location of the Hengill volcano in blue. [24] [15]

Along the Reykjanes Ridge, on the Reykjanes Peninsula are six major rift areas, also known as fissure swarms, of which the Hengill area is the most eastern one [24]. The Hengill Central Volcano lies at the triple junction between two active rift zones and a seismically active transform zone indicated with a blue dot on figure 2.1 (the Reykjanes Peninsula, the Western Volcanic Zone and the South Icelandic Seismic Zone) [15].

The volcano is mostly built up by hyaloclastite formations, formed by eruptions underneath the ice during the last ice ages, alternating with lava series from the interglacials [15]. The hyaloclastite formations consist of pillow basalts, breccias and tuffs. Most of the rock formations are basaltic in composition. Two main types of intrusions are found, fine grained basaltic intrusions and fine grained andesitic/rhyolitic intrusions, the intrusions are rare above 800m depth but are more common further down. A NE-SW striking fault swarm dominates the area, following the West Volcanic Zone, but easterly striking features are also present because of the intersection with the South Icelandic Seismic Zone [15].

Faults and fractures are the main fluid conducts in this area. Wells draw their hot water from these pathways, also known as feed zones [15]. A model built by Ratouis et al. [37] of the Hellisheiði field uses a permeability of 0.001 mD for the matrix and 152 mD for the fractures.

## 2.3. Well locations

Figure 2.2 shows the locations of the five fluctuating wells. The wells are located in two geothermal fields around the Hengill volcano, Nesjavellir in the north and Hellisheiði in the south. As the figure shows the fluctuating wells are not grouped in a certain location but are spread around the volcano.

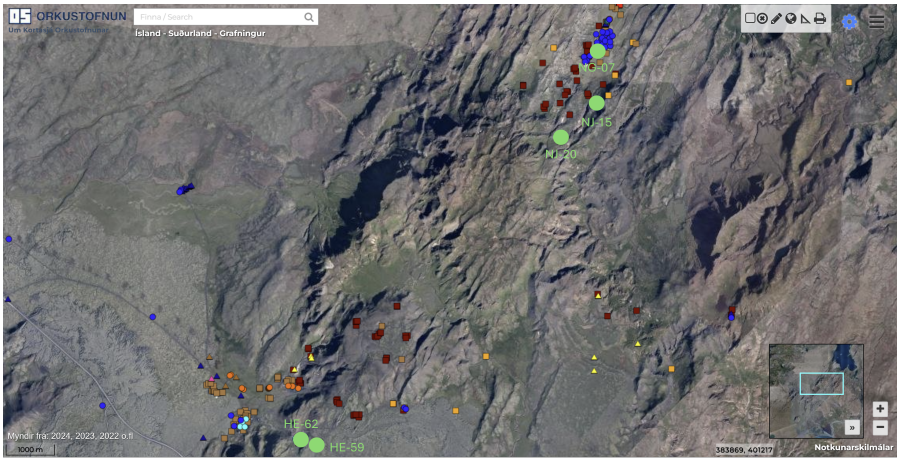


**Figure 2.2:** Locations of the five fluctuating wells show in green.[28]

The geothermal wells have a similar architecture. The main components of the wells are the casing and perforated casing (figure 2.3). The wells have casing for the first several hundred meters, this is a solid pipe preventing any inflow or outflow along the section. Each drilling phase the diameter of the pipes decreases as the new pipes have to fit through the ones already in place. After the solid casing is in place perforated casing follows, this is a pipe with holes along its length, allowing inflow of water but preventing large particles from entering the borehole and improving stability of the well bore. Figure 2.3 shows a schematic drawing of the casing in well NG-07 where there are three sections of solid casing decreasing in diameter and finally a perforated casing with the smallest diameter. The following two subsections will briefly state the casing depth and path of the five wells. Casing depth and path tell where the wells are sourcing the hot water from.

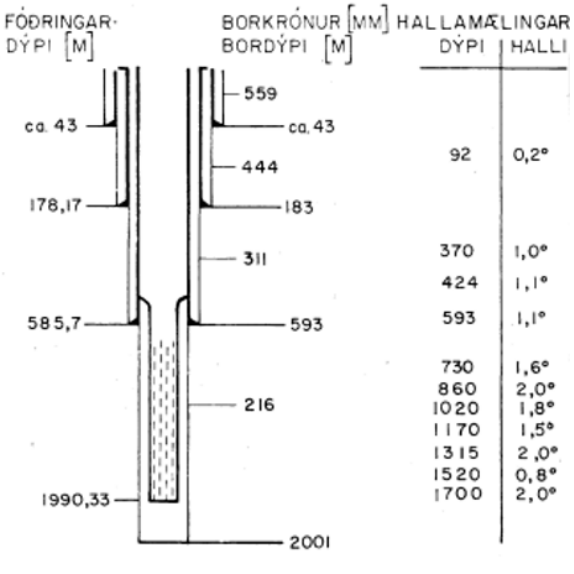


**Figure 2.3:** Casing diameter and depth for well NG-07 [9].

### 2.3.1. Hellisheiði wells

The two wells in Hellisheiði, HE-62 and HE-59 are about 350 m apart at the surface. However, they do follow very similar paths down as shown in Figure 2.4. They both cross the same fracture, indicated with a bold black line. Well HE-59 starts vertically and is deviated towards 252° after 350 m, casing goes down to 799 m deep and the perforated casing ends at 2381 m depth [18]. Well HE-62 also deviates after 350 m in the direction of 23 5°, casing reaches down to 795 m and the well has a perforated casing depth of 2260 m [42].

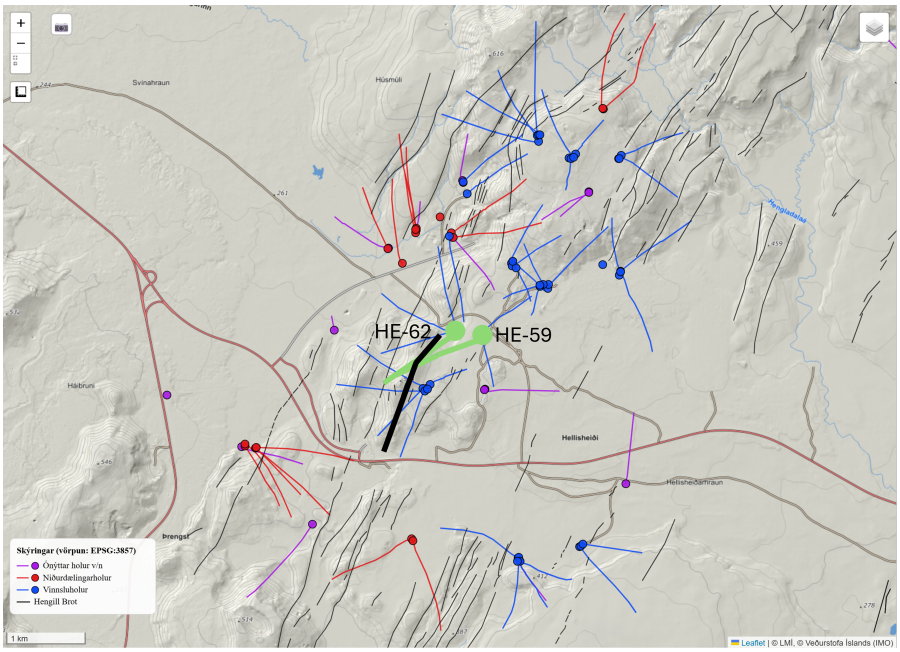


**Figure 2.4:** Locations of the fluctuating wells in Hellisheiði. Orkuveitan data base (2025).

### 2.3.2. Nesjavellir wells

The locations of the three wells in the Nesjavellir field are shown on Figure 2.5. Wells NG-07 and NJ-15 are vertical wells whereas well NJ-20 deviates from vertical after 334 m towards 220° [12] [13]. Casing for these wells is installed until 735 m for NJ-20 and a perforated casing depth of 1800 m [12], 790 m for NJ-15 and a perforated casing depth of 1722 m [43] and 585 m for NG-07 and a perforated casing depth of 1990 m [9].

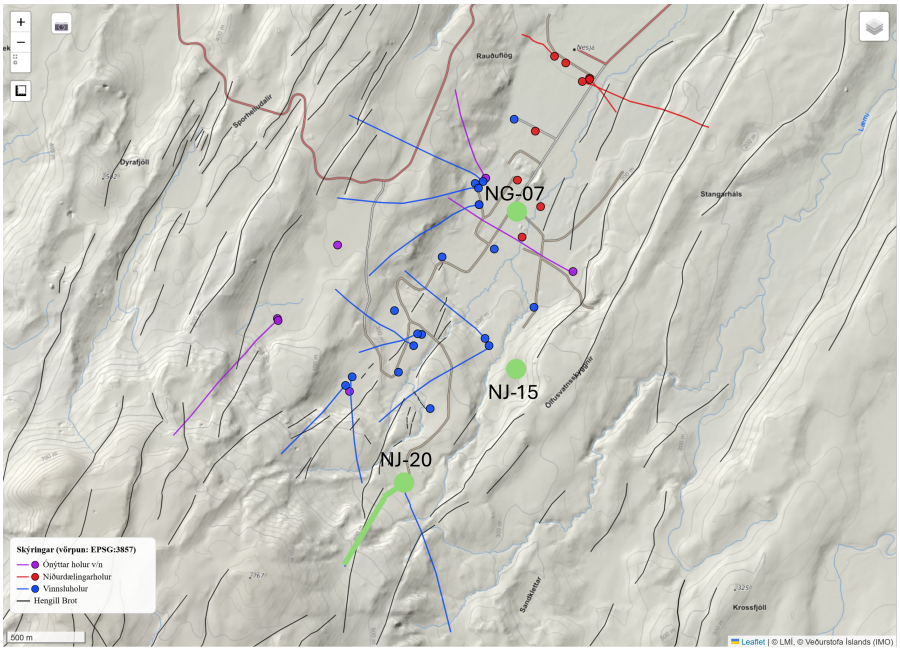


**Figure 2.5:** Locations of the fluctuating wells in Nesjavellir. Orkuveitan data base (2025).

## 2.4. Data overview

For each well we were provided with the technical reports and numerical data including:

- Drilling reports specifying depth, direction, casing depth, diameter, location of feed zones and geological units
- x, y and z coordinates of the wells, showing their surface location and path
- List of feed zone locations
- Wellhead pressure through time and if the well is open (in production), bleeding (small discharge to prevent pressure build-up), silencer (discharge into the atmosphere) or closed (no discharge at all)
- Pressure and temperature profiles along the well when it is closed
- Tracer flow testing data (including enthalpy, flow rate and pressure at the wellhead during production in time)
- Chemical data consisting of the composition of the vapour and liquid, ions and pH

All pressures are reported in bar-g, which corresponds to the measured pressure minus the atmospheric pressure. Apart from the five fluctuating wells we also got drilling reports, well head pressure data and PT data in depth as stated above for well NJ-14 and well NJ-31. These wells are operating normally with a stable well head pressure.

## 2.5. Pressure fluctuations

Time series data of the pressure at wellhead are available for all wells studied in this project. Figure 2.6 shows the pressure through time for well NJ-15 together with the condition of the well. When the

well is open, pressure fluctuations occur. However, when the well is closed, on silencer or bleeding the fluctuations stop (Figure 2.6).

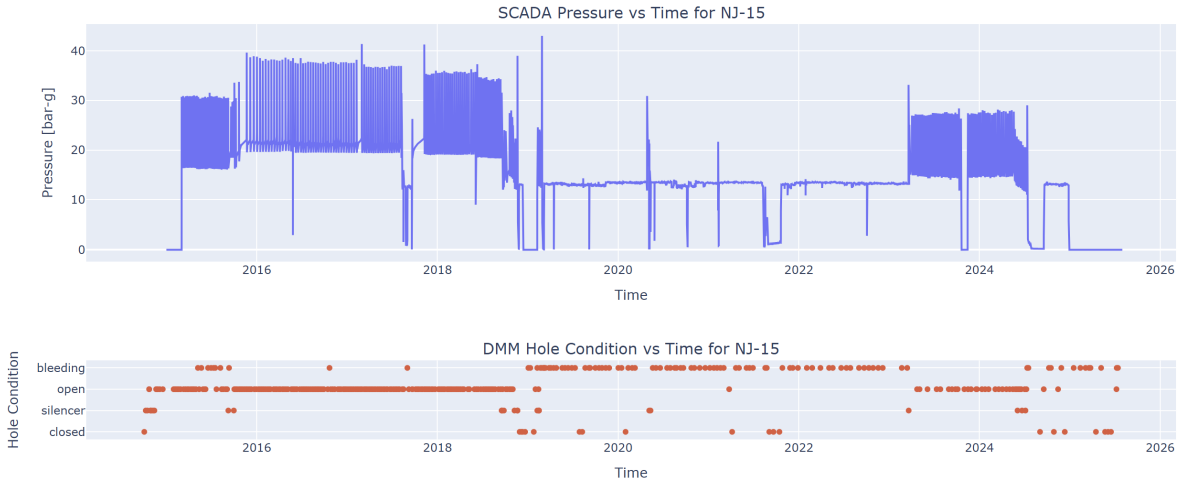


**Figure 2.6:** Pressure and hole condition for well NJ-15.

For each well, intervals with regular pressure fluctuations were selected to investigate the dominant frequencies. Figure 2.7 shows an example of selected intervals for well NJ-15.

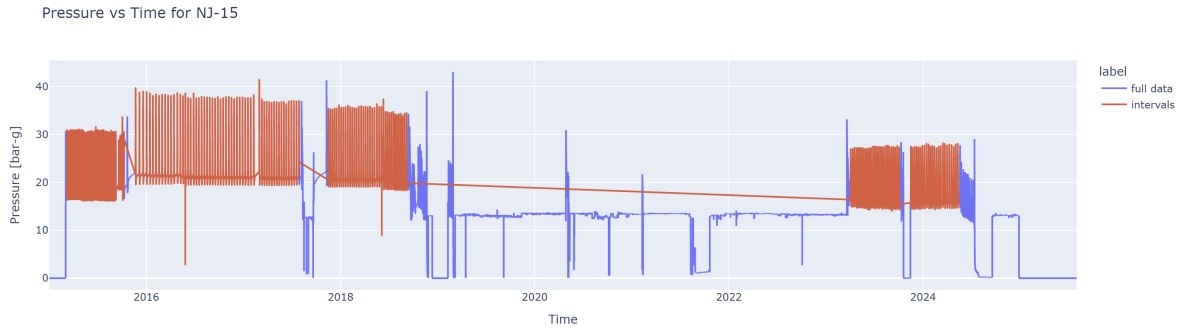


**Figure 2.7:** Selected pressure intervals for well NJ-15 in red.

Having isolated the intervals with regular pressure fluctuations, the frequencies of these intervals for each well have been calculated using Fourier transforms. As Figure 2.8 shows, the wells all have different frequencies and amplitudes for their pressure fluctuations, even the ones close to each other such as HE-59 and HE-62. For example, older wells such as NG-07, NJ-15, fluctuate every 6-10 days. Well NJ-20 fluctuating period varies from 10 days to up to a month. Newer wells such as HE-59 and HE-62, however, fluctuate every couple of hours.


**Figure 2.8:** Dominant frequencies on chosen intervals at the top and pressure fluctuations at the bottom.

Pressure and temperature logs of the wells at discrete times were also provided and plotted along with their feed zones, in Figures 2.9 and 2.10. The pressure and temperature measurements were recorded in depth every hundred metres. The more recently recorded profiles are plotted in lighter colours (yellow), while the older data is plotted in darker (blue) colours. These profiles were recorded between 1983 and 1997 at irregular intervals for well NG-07.

The temperature profiles vary in time due to the measurements being recorded both during and after drilling. The darkest measurements are taken during drilling and they show cooler temperatures because of the cold drilling fluid mixing with geothermal brine present in the reservoir. After drilling, the well warms up and the temperature logs shift to higher temperatures. These temperature logs do not follow a linear temperature gradient throughout the well, highlighting the impact of the different feed zones. The feed zones are classified into three categories: small, medium and large, and are plotted in green, orange and red respectively. These classes were attributed during the drilling process by considering pressure and temperature profiles, and drilling fluid loss. A relation between the classification of the feed zone classes and measurements of their size was not found in the provided data.

The pressure gradients are vertical near the surface, indicating the presence of water vapour and other gases. The pressure starts increasing after the steam-water contact and increases linearly, indicating hydrostatic water pressure.

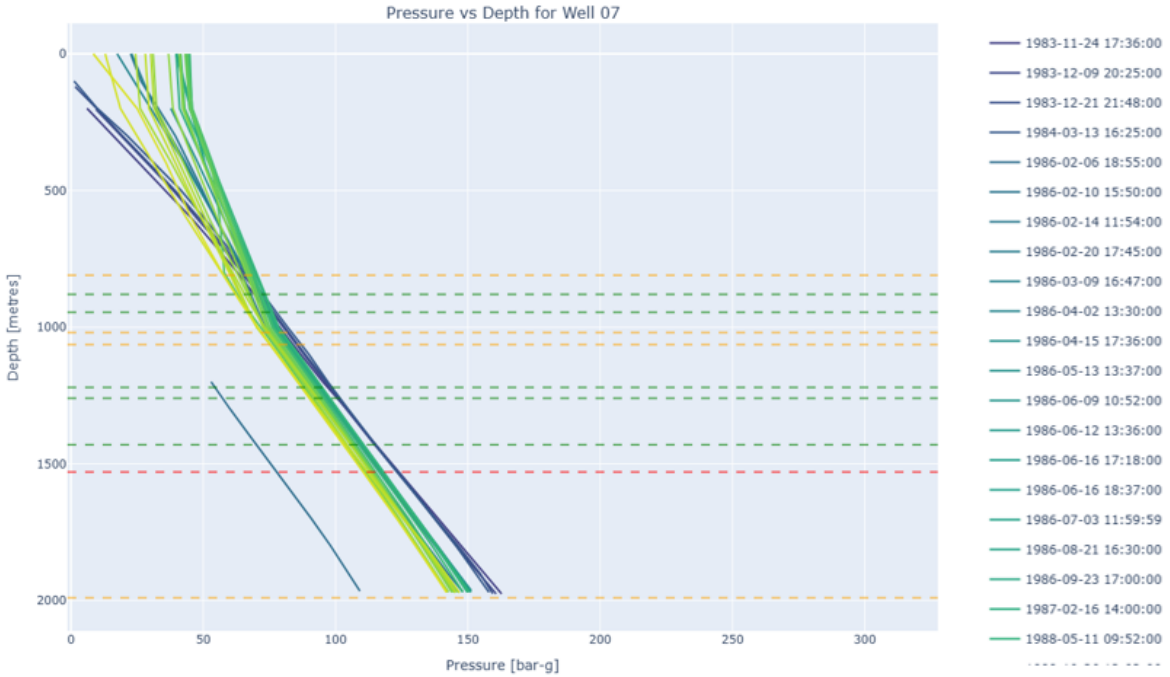


**Figure 2.9:** Pressure in Depth at different timestamps for well NG-07

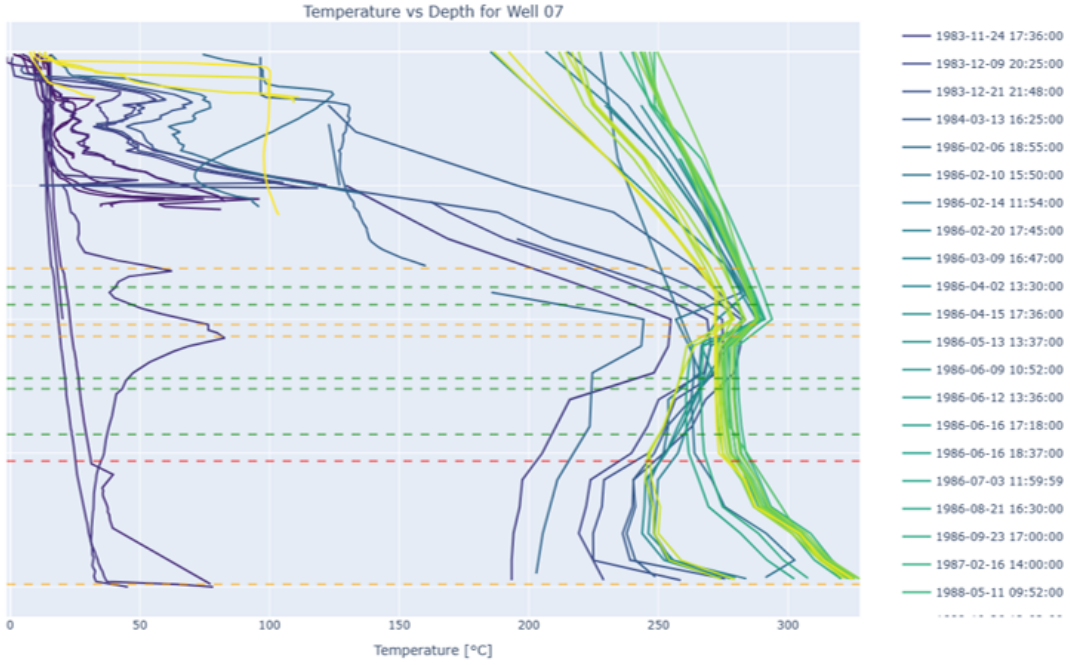


**Figure 2.10:** Temperature in Depth at different timestamps for well NG-07

# 3 Literature review

In this chapter, various hypotheses based on a literature review are discussed. Later, the most plausible hypotheses will be further explored in the Chapters 4 and 5. Section 3.1 explains the approach to the literary review, section 3.2 lists the hypotheses, gathered from the literature, which have been discarded, and section 3.3 introduces the most promising hypotheses that were chosen to be applied for this study. Lastly, section 3.4 explains the different types of models available to test the theories found in the literature.

## 3.1. Location of the origin of the pressure fluctuations

As stated in section 2.1 the geothermal well system consists of three parts: the reservoir, the well bore, and the infrastructure on top of the well. The first step is to find out where the fluctuations originate. Different locations in the systems have different mechanisms for causing fluctuations. In this section, the three components of the system and whether or not the fluctuations could originate there will be discussed.

### 3.1.1. Reservoir

First we consider if the fluctuations can be caused in the reservoir itself. According to Bjornsson et al. [5] the Hellisheiði and Nesjavellir fields are connected to the same upflow zone between the two fields but the connectivity between specific wells depends on the local fracture network. However, it does indicate that most wells are at least to some degree connected to each other. Fluctuations originating in the reservoir would occur in wells grouped together but in this case the fluctuating wells are spaced far apart. To further explore the impact of the reservoir we compared well NJ-20 (a fluctuating well) to well NJ-14 (a non-fluctuating well) and wells HE-59 and HE-62, two fluctuating wells next to each other.

Wells NJ-14 and NJ-20 are located only 46 m apart at the surface, see Figure 3.1. Well NJ-14 is a straight vertical well, while well NJ-20 bends away from well NJ-14 at depth. However, in both wells the feed zones are the two wells are tapping in the same reservoir. A direct comparison of the wellhead pressure data reveals that there are actually pressure fluctuation in both wells and at the exact same frequency (Figure 3.2), the only observable difference is the much smaller amplitude of the signal in well NJ-14. The effect on the productivity and flow rate of the NJ-14 well is negligible and therefore the well is considered to operate normally. Nevertheless, the origin of this artifact in the signal of well NJ-14 could be traced back to the pressure fluctuations originating in well NJ-20, due to the proximity between the two wells at the surface and the direct pipe connection between the well heads, as can be seen in the Figure 3.1. The signal is believed to communicate through the pipe network at the surface level rather than through the well because of the proximity and connection at the surface.

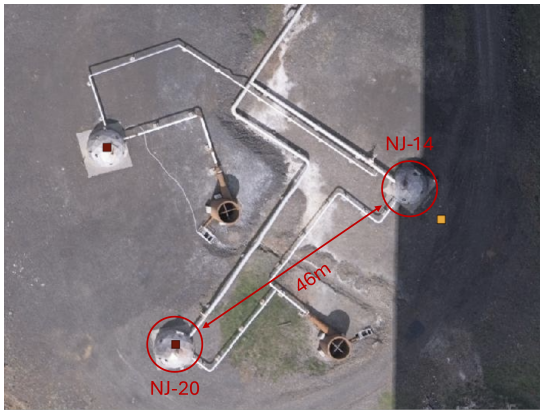


**Figure 3.1:** Locations of wells NJ-20 and NJ-14 at the surface. [28]

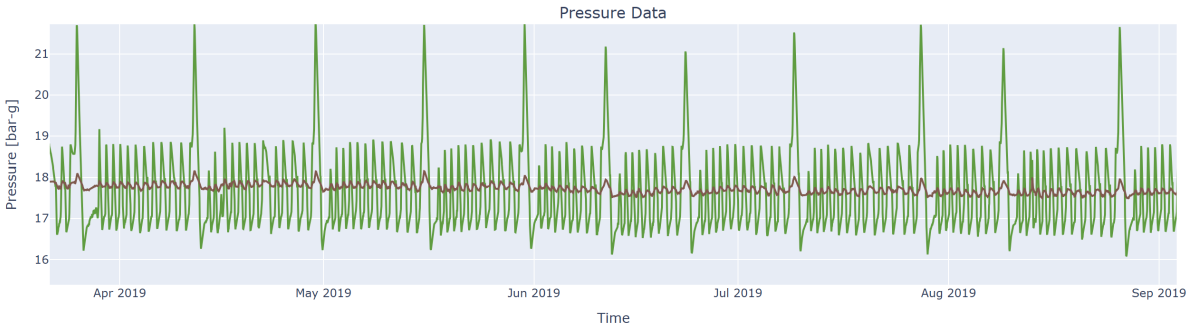


**Figure 3.2:** Pressure fluctuations in wells NJ-20 (green) and NJ-14 (brown).

Additionally, wells HE-59 and HE-62, as described in Section 2.3.1, tap into the same major fracture. However, they do show significant differences in fluctuation amplitudes and frequencies as shown on Figure 3.3. Although the amplitude mismatch could be explained by different well lengths and water volumes, the fluctuation frequencies would be expected to be the same for both wells if they originated within the reservoir.

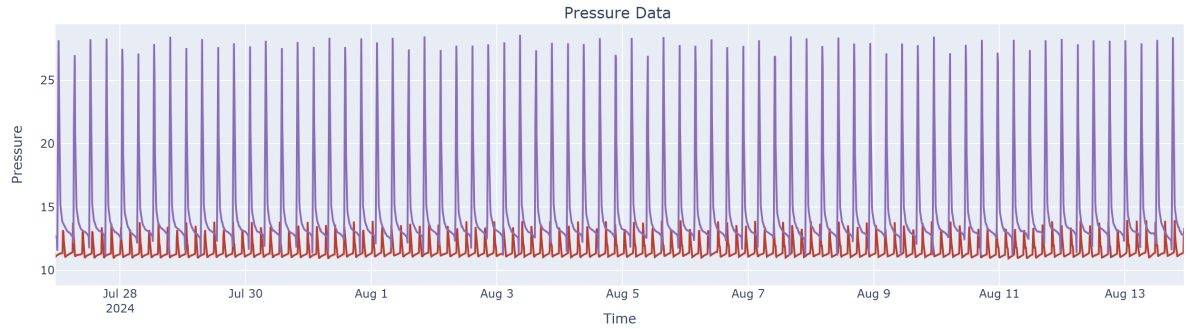


**Figure 3.3:** Pressure fluctuations in wells HE-59 (red) and HE-62 (purple).

Based on the fact that fluctuations only happen in a few wells spread throughout the entire area and that wells HE-59 and HE-62 appear to tap into the same reservoir but have different fluctuation frequencies we conclude that the fluctuations are not originating from the reservoir.

### 3.1.2. Infrastructure at the surface

The influence of the orifice plate and control valves of the wells were then investigated to determine if they could be at the origin of the pressure fluctuations. These are measures taken to control the flow rate at the top of the well, where the orifice plate has a fixed opening diameter the opening of the control valve can be adjusted during flow.

Well HE-59 has the most accurate data on the opening of the control valve, being recorded automatically every ten minutes. The period of the dominant frequencies of the wellhead pressure of well HE-59 were compared to the size of the opening of the orifice plate (Figure 3.4). A Pearson correlation correlation of 0.34 was calculated for the relation between periods and the opening of the control valve, using data intervals of 1 day. Using the same intervals, a Pearson correlation coefficient of -0.19 between the amplitude of the pressure fluctuations and the opening of the control valve was calculated. From these values, we were able to conclude that the opening of the orifice plate could have a small impact on the frequency of the oscillations, but close to none on the amplitude. As a result, it seems far fetched to associate these fluctuations solely with the opening of the control valve.

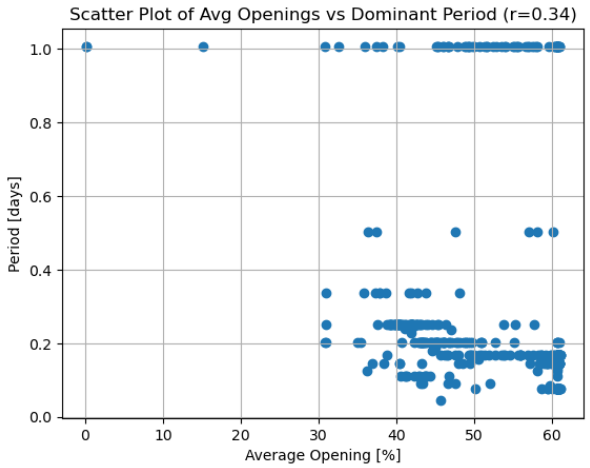


**Figure 3.4:** Scatter plot of the period of the dominant frequencies and the average orifice plate opening

The influence of the orifice plate was also considered. Orifice plates are used as cost-effective and permanent solutions to measure flow rates or control the flow from a well into the surface pipes [1]. In their model to evaluate the two-phase flow rate at an orifice place, Helbig and Zarrouk [17] conceive a model in which the gaseous phase in the tube momentarily stops the liquid phase from flowing through the orifice plate. The liquid phase then stops, accumulates, and eventually passes through the orifice. This small accumulation could then cause a noticeable fluctuation in the pressure sensor at the well head. However, no clear frequency in the changes in mass flow rate could be seen in measurements at the orifice plate from Helbig and Zarrouk [17], making it unlikely that the orifice plate would be the origin of periodic pressure fluctuations. Additionally, all 72 geothermal wells around the Hengill Volcano use orifice plates and only five of them show fluctuations.

In summary, the orifice plate can cause small fluctuations in pressure at the well head, but it does not cause the as large periodic fluctuations as observed in the fluctuating wells. From this, we concluded that the pressure instabilities in the well were not caused by the infrastructure at the well heads.

### 3.1.3. Well bore

Having considered the reservoir and top hole infrastructure and concluded that neither is likely to be the origin of the fluctuations, the well bore is the last option left. We did not find any evidence opposing the theory that the fluctuations originate from the well bore or near-wellbore region. We therefore concluded that the observed pressure oscillations must be the result of thermodynamic or fluid-dynamic effects occurring inside the well, rather than in any other part of the system.

## 3.2. Discarded theories from literature

As described in section 3.1 the pressure fluctuations are most likely not caused by a problem in the reservoir itself, since the reservoirs appear to be interconnected. Therefore, the cause of the problem must be inside the well or in the near-wellbore region. The literature provides a number of theories that can act as a trigger for unintended pressure fluctuations at the well head. This section will briefly describe the hypotheses considered for this project, which were briefly looked into, but disregarded soon after due to these mechanisms being improbable to cause fluctuations for various reasons.

### 3.2.1. Natural geysers

The observed pressure fluctuations remind one of the behaviour of a geyser, a natural phenomenon commonly found in the region. Geysers have rather complex underground structures that are not yet fully understood [27]. There are two conceptual models to explain the main mechanism in geysers [21]. One describes steam trapped in an underground cavity and the other ascent-driven decompression and subsequent boiling of the fluid in the conduit. The conduit generally has a constriction near the top [22]. Each mechanism will be described in the following paragraphs.

The mechanism of natural geysering involves proximal underground cavities that are located next to the main conduit. These so called 'bubble traps' are filled with non-condensable gas or superheated vapour [39]. Once the total volume of gas exceeds a certain threshold, it starts to push up the liquid in the conduit, causing an eruption.

The flash-boiling mechanism occurs in the conduit itself. At the top of the conduit the temperature is equal to the boiling temperature of pure water, further down the conduit the temperature lies below the hydrostatic boiling temperature [21]. As the eruption draws closer, the boiling point (flash point) in the conduit propagates downward. The buoyant superheated water is convected upward, leading to the formation and expansion of steam bubbles as the pressure drops. The down flow occurs mainly on the sides of the conduit; as the temperature increases, more bubbles rise up through the centre and expand until frictional resistance suppresses convective down flow, leading to an eruption.

Natural geyser systems studied to date generally reach only a few tens to hundreds of metres depth. The tallest active geyser in the world, the Steamboat in Yellowstone National Park, has a conduit that reaches 120 m depth [47]. Strokkur, a geyser in the same region in Iceland, has its bubble trap at 25 m depth and its groundwater reservoir is located at 150 m depth [27]. The wells studied for this report have casing that extends to a depth of 800 metres, meaning that possible bubble traps must be located below the casing at much deeper levels than in any known natural geyser. The casing in the well bore also means there are no constrictions in the conduit. Additionally, the lack of high resolution geological and geophysical data around the wells means the theory cannot be verified. Consequently, the natural

geyser theory was discarded.

### 3.2.2. Gas expansion

In New Zealand, a team of researchers analysed geothermal wells that are 'geysering', where water and gas erupt in an oscillating pattern from the well. After the eruption, the cycle continues with the water level dropping below the exposed surface for a period of time until the water recharges, the water level starts to rise again and the cycle repeats [26].

The geysering effect in the geothermal well in New Zealand is caused by the dissolution and consequent degassing of carbon dioxide from the water in the well [26]. Initially, carbon dioxide is fully dissolved in the reservoir. The water rises inside the well bore and starts to degas as a result of the decrease in pressure, releasing increasing amounts of gaseous carbon dioxide while travelling up. At the beginning of the cycle described by Lu et al. [26] the water level in the well increases until the rim of the well. Water starts flowing over it and simultaneously releases small gas bubbles into the air. Gradually, the overflow becomes continuous as the water level rises slightly above the wellhead with an increase in gas bubbles observed in the water. As more gas escapes into the open air, the water flow becomes intermittent until fluid starts to be ejected along with the gas from the wellhead in a series of eruptions that occur in rapid succession. When the eruptions end, the water level is well below the wellhead again and the geysering cycle repeats.

Figure 3.5 shows the temperature and pressure measured at a depth of 20 metres in the well bore during a geysering cycle. Time A is the moment the water level reaches the wellhead, this is also the time when the pressure reaches its maximum while the temperature is at its minimum [26]. As the well continues to overflow and more bubbles appear, the pressure drops and the temperature rises. At time B the first eruptions start, due to the high gas concentration in the gas-liquid mixture. The pressure is at its lowest at this point while the temperature is still rising. After time C the eruptions have ceased and the water level is below the wellhead again. Between times C and D, the pressure at 20 metres depth starts to increase again as the well is recharging from the bottom of the well, triggering a new episode of degassing inside the well bore. As the gas travels up the well faster, between times D and E, mainly liquid without gas bubbles rises, causing a near-linear pressure increase.

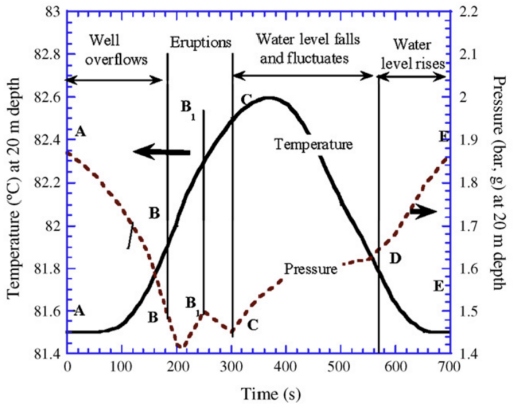


**Figure 3.5:** Pressure and temperature throughout one geysering cycle. [26].

Lu et al. [26] created a numerical model that found that the main controls of geysering in the well are the

mass inflow rate from the reservoir and the concentration of carbon dioxide in the geothermal fluid. By increasing the mass inflow rate or reducing the carbon dioxide concentration, geyser behaviour can be successfully suppressed [26]. Well engineering solutions to achieve this could be realised by a reduction in the diameter of the well to decrease the overall flow rate or by altering the chemical composition of the geothermal fluid (e.g., by injection of liquid or chemicals that alter the solubility of carbon dioxide in the fluid) to actively control the carbon dioxide concentration.

Ultimately, this theory was discarded because of the nature of the well in the study by Lu et al. [26] is hardly comparable to our wells on the Reykjanes peninsula. Although the amount of carbon dioxide is found to be at similar concentration levels, the well that was modelled for this study is much shallower (70 metres depth) than the wells studied for this report and operates at much lower temperatures, as the water produced continuously stays below the bubble point. Additionally, our wells contain many other non-condensable gases, such as $H_2S$ and $CH_4$ among others, with different solubilities. When comparing these numbers with the diameters and volumes of fluid inside of the high-enthalpy wells at Reykjanes, the amount of degassing carbon dioxide appears to be too low to be the only trigger of geysering behaviour. In this study, the effect of other degassing compounds on geysering in the Icelandic wells could not be determined. However, as Icelandic wells operate at much higher temperatures, pressures, and flow rates, we assume that the main contributing phenomenon in our wells must be of thermodynamic or fluid-dynamic nature.

## 3.3. Applicable theories from literature

**Multiple Feed Zones Theory:** As mentioned in the section above, pressure fluctuations in geothermal production wells have been observed in previous cases. A team of Japanese researchers, Yamamura et al. [48] analysed the behaviour of well-head pressure oscillations during the operation of high-enthalpy geothermal wells with multiple feed zones. In this study, the researchers described the phenomenon of geothermal brine rising from a large hot feed zone at the bottom of the well, eventually reaching two-phase flow conditions on its way upward. Later, single-phase liquid enters the well from shallower feed zones, creating multiple areas with unstable conditions where flash boiling and rapid phase changes occur within the well [48]. The geological and thermodynamic conditions of their concept of competing feed zones seem to be very similar to those present in our wells, as both situations involve high-enthalpy geothermal fluid and multiple feed zones.

**Internal Flow Instability Theory:** Another type of oscillating phenomenon has been experienced in other high-enthalpy geothermal wells [41]. This phenomenon is expressed by cyclic transitions in flow patterns inside the well bore that cause pressure drops and are usually triggered by continued random shifts in the external characteristics of the system, such as mass flow rate and enthalpy [40]. This behaviour can occur if the system's characteristic curve of pressure drop vs. mass flow rate shows an instability condition, resulting in a negative slope, a criterion defined as Ledinegg instability [25, 40]. We initially approach this problem by comparing it with the 'heading' phenomenon, which can occur under similar circumstances in gas-lifted oil wells [16].

Chapter 4 analyses the required conditions of the characteristic pressure drop vs. flow rate curve for Ledinegg instability and explores cyclic transitions in the two-phase flow and its effects on pressure output and flow rates by comparing it to flow pattern transitions occurring during the heading

phenomenon in gas-lifted oil wells. Chapter 5 expands on the mechanism of the multiple feed zones theory, where the interplay of well bore feed zones creates oscillating pressure and flow rate.

## 3.4. Available models for two-phase flow

Both of the proposed theories, the Internal Flow Instability theory and the Multiple Feed Zones theory, require detailed modelling of two-phase flow. For this, a type of model is chosen which honours the necessary granularity, without becoming too complex to be applied to the problem. Ultimately, we want to realistically model the two-phase turbulent flow of liquid water and steam for the well bore system, given the limited amount of data and the number of available input parameters. Among researchers, three stages of model complexity are being used in the simulation of two-phase well flow. Homogeneous flow models, separated flow models, and flow-pattern models [16]. All these models are based on the standard equations for the conservation of mass, momentum and energy [19].

The simplest approach to modelling two phase flow is a homogeneous flow model. This model treats the two-phase flow as a phase mixture, assuming the same average flow velocity and thermal phase equilibrium for gas and liquid throughout the pipe section, without distinguishing between flow patterns in the phases or accounting for slip [19]. This type of model provides reliable averaged results to calculate the basic conditions for the occurrence of internal instability and representatively simulate the pressure drop in the well [16]. With the simulation of Matsumoto et al. [29] in Section 5.4 we employ a homogeneous flow model to simulate our well bore conditions for the Multiple Feed Zones theory. However, this simplistic model becomes increasingly insufficient for modelling vertical well bores, where gas tends to travel at speeds significantly higher than the liquid phase [31, 16].

To account for this problem, separated flow models with higher complexity were employed in parts of our research, where modelling as a single phase mixture fluid does not honour the required detail. This was the case for two of the three models used in this study; we first used STARS, a thermal reservoir simulator model developed by the Computer Modelling Group (CMG) to verify if the required conditions to trigger pressure fluctuations were met, within the Multiple Feed Zones theory. For the detailed methodology behind this approach, please refer to section 5.3. We then confirmed the results of the STARS model using the simulation of Matsumoto et al. [29]. Finally, we used our own model, as described in section 4.2, which was used to investigate the Internal Flow Instability hypothesis. Both of these theories require one to account for slip between the two phases making use of separated flow models.

Separated flow models such as STARS aim to simulate each phase individually. In the same way as homogeneous flow models, they are based on conservation equations, with the difference that these are now applied and calculated for each phase individually [19, 16]. To include information on the forces present along the phase boundary and on how the two phases interact with each other, additional terms that describe this interaction are included [19]. Further terms are required to simulate the exchange of mass, momentum and energy between the two phases, which relate to different flow velocities and consequently occuring shear and drag forces among the individual phases [19].

The currently highest stage of complexity in two-phase flow modelling is reached by models that simulate actual flow patterns [16]. Nevertheless, a definitive prediction of the exact flow pattern and their transitional phases is still hardly achievable due to the non-linear behaviour of the forces involved

[31]. Especially during the transition from one pattern to another, the factors that determine the form of the resulting flow pattern are numerous and highly variable, depending on operating conditions, changes in fluid viscosity, liquid and steam production rates, temperature and enthalpy, as well as roughness of the tubing, pipe orientation, and casing shape, among many others [31]. This type of model has been discarded for this study, as it is impractical for our case due to the limited data available and its high complexity, which was beyond scope and not required for our type of research. Furthermore, commercially available models of this grade are scarce, require many input parameters and computational capacity, and are very expensive.

# 4 Internal Flow Instability Theory

This chapter focusses on our hypothesis based on the phenomena of Ledinegg instability and pressure drop oscillations accompanied by cyclic changes in flow patterns. We illustrated this hypothesis by comparing it to the phenomenon of 'heading', an oscillating behaviour that can occur in gas lifted wells operating under two-phase flow conditions [16]. The occurrence of heading has been intensively studied for the production of natural gas and oil, for example, by Duns and Ros [8]. In geothermal wells the instabilities in the two-phase flow are driven mainly by changes in the relationship between the internal and external pressure drop of the system [41]. Both phenomena are self-excited and self-sustaining oscillations due to delayed feedback between flow and pressure states in multiphase flow systems that can occur if there is a sufficient amount of compressible volume (gas or steam) inside the well [40].

Section 4.1 describes the theory behind the internal flow instability, section 4.2 will describe the methods used to test this hypothesis, and finally section 4.3 will present the findings related to this hypothesis.

## 4.1. Literature

The approach towards the described hypothesis is two-fold, as internal flow instability and oscillating flow pattern transition can occur in various heated and non-heated multiphase flow systems including high-enthalpy geothermal wells and gas lifted oil wells [16, 41, 40, 8].

**Gas-lifted oil well:** In gas-lifted oil wells, 'heading' is a common consequence of oscillating unstable flow states where liquid hold-up occurs in certain sections within the well, which can lead to increased accumulation of liquid, known as liquid loading [8, 2]. Liquid hold-up and consequent liquid loading are triggered by an insufficient in-situ flow velocity of the liquid phase ($v_{SL}$) in relation to the gas phase ($v_{SG}$) within the tubing, which creates a difference in the in-situ flow velocity between the two phases, called slip [16, 45]. This difference in in-situ flow velocities allows the liquid phase physically to lag behind the gaseous phase on its way travelling up the well, initiating an unintended build-up and continued accumulation of liquid inside the well. The slower moving water droplets easily coagulate and form a continuous phase that tends to be dragged along upward with the faster-moving gas phase. The liquid phase then wraps around sections of the inner walls of the production casing at high gas production rates, creating the characteristic annular flow pattern [16]. In this flow pattern, nearly all the gas surpasses the accumulated liquid in the centre of the casing as can be seen in Figure 4.1.

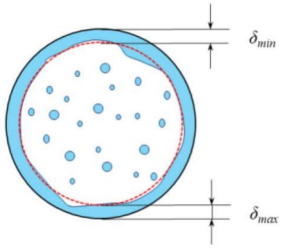


**Figure 4.1:** Liquid and gas distribution in the well bore during annular flow pattern. [36]

During this flow state, sudden random changes in the flow velocity or volume of the gas phase can cause a reversal of the liquid film and consequently lead to sudden bridging of the annular liquid phase through the centre of the well [3, 19]. This leads to temporary obstructions of the gas flow in the well, as illustrated in figure 4.2, and the two-phase flow becomes intermittent. A slug or plug flow pattern evolves.

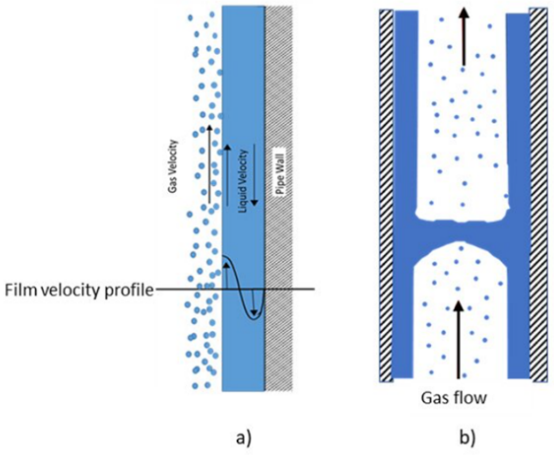


**Figure 4.2:** Reverse liquid flow creates local instabilities in the liquid film and initiates the appearance of bridging and intermittent flow, which can lead to oscillating internal flow instabilities [3].

This situation is self-induced by the system and will potentially develop an oscillating behaviour of repeating transitions in the flow patterns, as seen in figure 4.3, if a continuous feedback loop is established between gas accumulation, pressure increase, sudden discharge, and liquid accumulation [3, 19, 40]. This oscillating behaviour is called heading and produces large non-damped continuous flow rate and pressure oscillations as seen in Figure 4.4 that appear to look fairly similar to the fluctuations observed in the Icelandic wells.

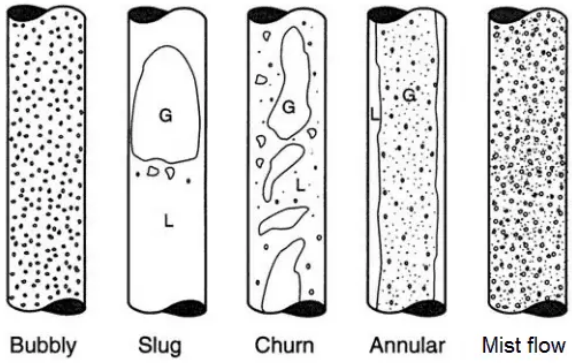


**Figure 4.3:** Overview of different two-phase flow patterns in vertical wells. [7]

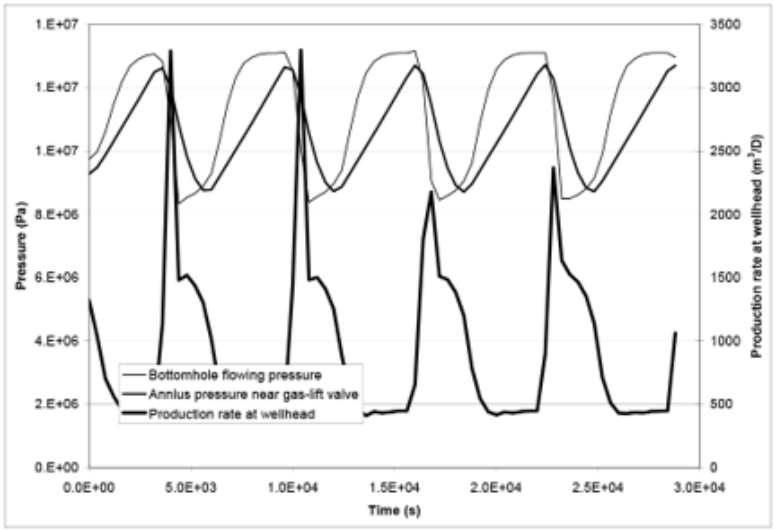


**Figure 4.4:** Pressure and flow rate oscillations related to heading in a gas-lifted oil well. [20]

**High-enthalpy geothermal well:** An analogous oscillating behaviour can be observed in vertical boiling channels, such as high-enthalpy geothermal wells which are called 'pressure-drop oscillations' [40, 41]. In contrast to the heading phenomenon, pressure-drop oscillations are caused by instabilities in the internal pressure-drop gradient which can be a result of small changes in the phase flow velocities caused by variations in mass inflow, sudden flash boiling or bottom hole pressure [40]. This 'Ledinegg instability' or 'flow excursion' describes a macroscopic static flow instability that occurs in boiling or flashing two-phase systems where a small perturbation in flow rate causes the system to jump to another equilibrium [25, 40]. This condition relates to the left branch of the characteristic curve of internal pressure drop vs. flow rate of the system, as shown in Figure 4.5, which has a negative slope, indicating the instability region at low mass flow rates. The Ledinegg-type instability therefore provides the static condition required for the consequent onset of a dynamic instability,the so called 'pressure drop oscillations' [40].

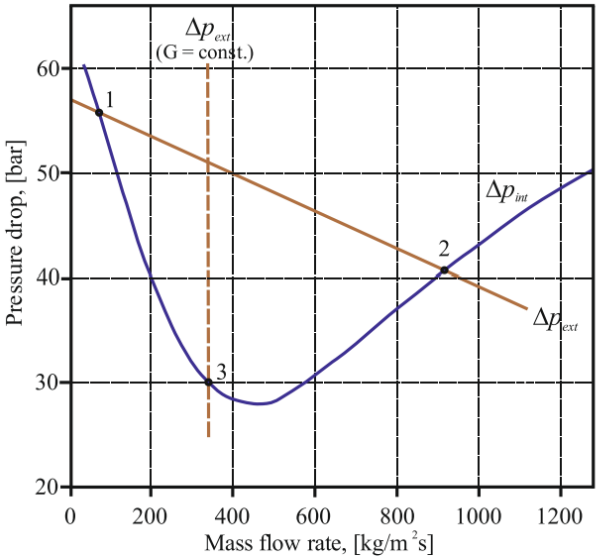


**Figure 4.5:** 'Internal and external pressure drop vs. flow-rate characteristic curves for [a] steam-water geothermal well' [41].

This type of oscillation is self-sustaining on the basis of energy conservation, as energy is cyclically exchanged at the phase boundaries between the compressible volume and the fluid inertia. In high-power-density systems, such as steam producing geothermal wells, only a small compressible volume is needed to sustain these oscillations [40, 41].

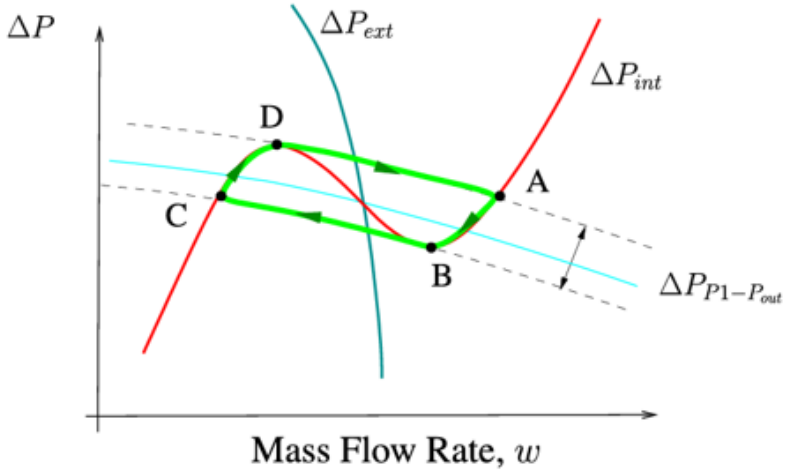


**Figure 4.6:** Shifting external characteristics condition [40]

The oscillations that can occur in geothermal wells are characteristic of four different phases within one cycle that represent a classic thermodynamic circular process as can be seen in Figure 4.6:

In the initial compression phase (CD), the flow decreases, the steam collapses, condenses, and the density increases, while the pressure at the wellhead increases (charging the compressible volume). Next, the flow rate drops far enough that flashing nearly ceases, and the well behaves as it was liquid-dominated, leading to a flow excursion to single-phase (DA). Subsequently, the pressure in the wellhead drops as the compressible column expands, triggering a flow acceleration in the decompression phase (AB). As an immediate result, rapid and sudden flashing occurs, coinciding with a sharp increase in the void fraction and an increasing pressure drop, which leads to another flow excursion to a high-quality two-phase flow (BC) again and the cycle restarts [40].

These pressure drop oscillations have been observed in geothermal wells in Russia, where a continuous periodic exchange between compression and inertia is regulated by two-phase dynamics [41].

A repeating pattern of flashing, changes in void fraction, and flow velocities, involving cyclic transition between different flow patterns, can only occur after enough liquid has accumulated through liquid film reversal, around the walls of the piping, or (for geothermal wells) after sufficient heating of the vertical boiling pipe [40]. It is therefore common that heading in gas-lifted oil wells and pressure-drop oscillations in geothermal wells occur only after the well has been operating normally for a certain amount of time. Once the periodic oscillations are established, they become self-sustaining, due to constant changes in the systems external stability.

While heading in gas-lifted oil wells is caused by upstream compressible gas volumes and flow rate fluctuations, pressure drop oscillations in vertical boiling pipes, such as geothermal wells, relate to non-monotonic intervals of the pressure drop vs. mass flow curve (Ledinegg criterion) [2, 36, 40].

Nevertheless, the consequences of these two phenomena to the system are the same.

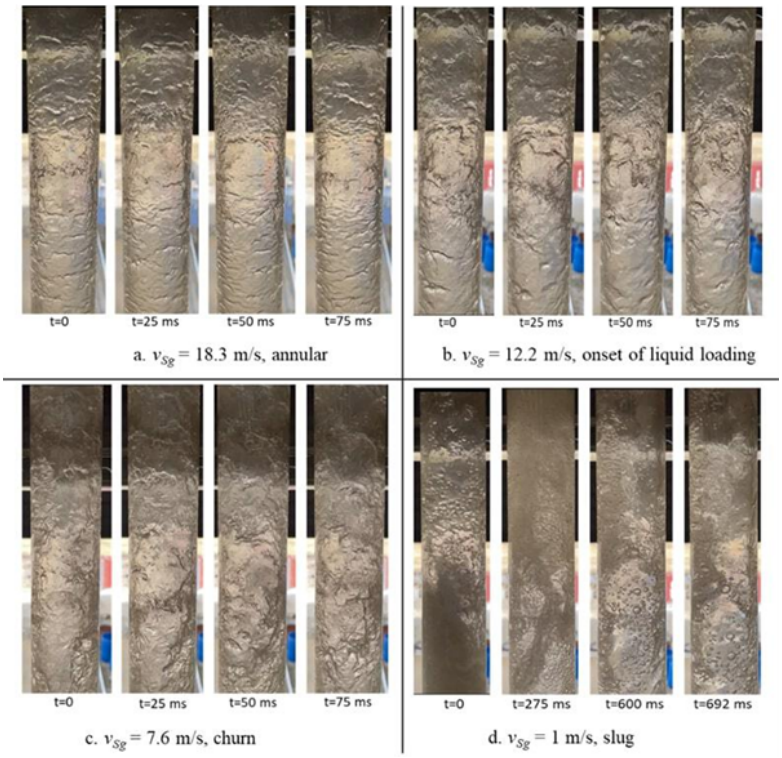


**Figure 4.7:** 'Snapshots of different flow patterns [...] for $v_{SL}$ = 0.01 m/s [...]' [2].

The sudden change in pressure and flow rate also affects the flow velocities of the individual phases. This change in slip is accompanied by transitions in the flow pattern, as seen in Figure 4.7, depending on the difference in flow speed between the two phases. This sends a pressure shock wave in both directions up and down the well, amplifying these fluctuations throughout the whole well system [45].

The fluctuations can be measured throughout the well, but are usually recorded at the bottom hole and the well-head. As can be seen in Figure 4.4, the fluctuations in a gas-lifted oil well appear to show a pattern similar to the oscillations that we observed at the well head of the Icelandic wells. After the in-situ flow velocities of the gas and liquid phases have stabilised again, the system returns to the annular flow pattern and the cycle repeats.

The probability of heading in a well operating under two phase conditions has been found to increase with a lower velocity of the liquid phase and higher gas phase velocities and consequently a larger slip between the two phases [8].

## 4.2. Methodology

Let us consider the momentum balance of a point along the well bore, expressed as Newton's second law. In it, we present well head pressure ($WHP$) as the sum of bottom hole pressure ($BHP$) and internal pressure changes -namely gravitation, friction and acceleration losses.

$$WHP - BHP - \frac{dp}{dz}_{grav} - \frac{dp}{dz}_{fric} - \frac{dp}{dz}_{acc} = 0 \tag{4.1}$$

Now, let us suppose a small disturbance in momentum caused by a change in mass flow rate $\frac{d}{d\dot{m}}$. An increase in flow rate will not amplify instabilities if it causes a decrease in momentum along the well -i.e. flow will remain stable if an increase in flow rate causes a reduction of the forces. Shulyupin [41] describes the stability of similar geothermal wells as:

$$\frac{d}{d\dot{m}}\left(WHP - BHP - \frac{dp}{dz}_{grav} - \frac{dp}{dz}_{fric} - \frac{dp}{dz}_{acc}\right) < 0 \tag{4.2}$$

Where the first two describe the pressure changes on either side of the well (bottom and top hole), and the last three those occurring inside the well bore. Therefore,

$$\Delta p_{ext} = WHP - BHP \tag{4.3}$$

and

$$\Delta p_{int} = \int -\left(\frac{dp}{dz}_{grav} + \frac{dp}{dz}_{fric} + \frac{dp}{dz}_{acc}\right) \cdot dz \tag{4.4}$$

We can thus present the stability condition 4.2 as:

$$\frac{d\Delta p_{int}}{d\dot{m}} > \frac{d\Delta p_{ext}}{d\dot{m}} \tag{4.5}$$

Equation 4.5 is known as the Ledinegg stability condition, classified as a macroscopic and static (in)stability (Ruspini et al., 2014, p. 523 [40]).

According to Ruspini, Marcel, and Clausse [40], 'in most practical cases this situation will never happen, since in operation conditions it is not possible to achieve a static unstable point' (p. 524). If this happens, the operating conditions will migrate to a new stable point -known as a flow excursion. However, there are cases where an excursion can cause a change in another parameter (e.g. void fraction); causing, in turn, the operating conditions to cycle between unstable points. This behaviour can lead to irregular flow and fluctuations.

In our model, the $WHP$ is kept constant -$WHP$ data fluctuates around a constant value, as discussed later. Therefore, the change in external pressure will rely entirely on $\frac{d}{d\dot{m}}BHP$. Later in this section, we will define this as $\frac{d}{d\dot{m}}\Delta p_{ext} = J^{-1}$ (see Eq. 4.8 and Figure 4.8).

Intuitively, this value will always be negative: since drawing more fluid from the reservoir will lower the pressure in the near-bore region (Shulyupin, 2016, p.291 [41]). Therefore, following Equation 4.5, a well will be stable if:

$$\frac{d\Delta p_{int}}{d\dot{m}} > 0 \tag{4.6}$$

This equation describes the Ledinegg stability across the entire length of the well $\Delta z$. Moreover, the stability can also be assessed along the well bore, if a smaller increment $dz \rightarrow 0$ is considered. Condition 4.6 then becomes:

$$\frac{d}{d\dot{m}}\left(-\frac{dp}{dz}\right) > 0 \tag{4.7}$$

In this section, we describe a numerical modelling approach to Equations 4.6 and 4.7. Our aim is to model and compare the characteristic curves of a stable and unstable well, i.e. the relation between mass flow rate $\dot{m}$ and pressure drop $\Delta p$.

For this, we will perform a nodal analysis, following the workflow described by Jansen [23].

A nodal analysis describes a production system analogically to an electrical circuit with resistors in series, where the properties of the fluid are evaluated at each step.

Here, we limit our study to a configuration that includes three steps: reservoir, bottom hole and well head. The relation between mass flow rate $\dot{m}$ and internal pressure changes $\Delta p_{int}$ will be calculated at each step, to arrive at a final expression that can be used to assess Eqs. 4.6 and 4.7.

In the first three subsections (§ 4.2.1 - 4.2.3), the theoretical framework of flow in a well will be described, using the corresponding governing equations. In subsection § 4.2.4, the boundary conditions and constants of the numerical model will be determined. Subsection § 4.2.5 will discuss the discretization scheme of the numerical model. Lastly, section 4.3, will present the output of the model. A combined discussion of both hypotheses will follow in a separate chapter.

### 4.2.1. Inflow Performance

The first step is to calculate the bottom hole pressure $BHP$ as a function of mass flow rate $\dot{m}$ and reservoir pressure $p_{res}$. As outlined in Jansen [23], this can be described by the Inflow Performance Relation:

$$BHP = p_{res} + \frac{\dot{m}}{J} \tag{4.8}$$

where the productivity index $J\left[\frac{kg}{Pa \cdot s}\right]$ is expressed as a function of (liquid) viscosity $\mu_l$, density $\rho_l$ and well radius $r$:

$$J = \frac{2 \cdot \pi \cdot kh \cdot \rho_l}{\mu_l \cdot \ln(\frac{r_e}{r})} \tag{4.9}$$

The permeability $k$ of the reservoir is estimated to be around 10 mD (Bodvarsson et al., 1988, p.89 [6]), throughout the length of perforated casing ($h$ =1400 m). As a result, $kh = 1.4 \cdot 10^{-11}\ m^3$. The value for reservoir radius $r_e$ was taken somewhat arbitrarily from Yamamura et al. [48] as 1000 m.

NB. It was assumed that the reservoir operates in a liquid only flow into the tubing. As seen in Figure 4.8, bottom hole pressures always remain above the bubble point.

The results from this calculation are presented in said Figure, in the next section.

### 4.2.2. Tubing performance: Single Phase Flow

In the next step, we will calculate the internal pressure drop $\Delta p_{int}$ along the well bore.

We will start with the continuity equation for conservation of mass:

$$\frac{d}{dz}(\dot{m}) = 0 \tag{4.10}$$

As previously seen in Eq. 4.4, the conservation of momentum in steady state can be written as the sum of gravity, friction and acceleration (sometimes inertial or kinetic) pressure losses (see Jansen, 2017 [23] or Guðmundsdóttir, 2012 [11]).

$$\frac{dp}{dz}_{int} = -\frac{dp}{dz}_{grav} - \frac{dp}{dz}_{fric} - \frac{dp}{dz}_{acc} \tag{4.11}$$

Let us consider the case for liquid only flow in a well. The momentum balance can be expanded into:

$$\frac{dp}{dz}_{int} = -\rho g \sin(\theta) - \frac{f\rho}{4r}\, u\,|u| - \rho u \frac{du}{dz} \tag{4.12}$$

where the velocity of the fluid $u\ \left[m/s\right]$ is:

$$u = \frac{\dot{m}}{\rho A} \tag{4.13}$$

Substituting Eq. 4.13 into Eq. 4.12 gives:

$$\frac{dp}{dz}_{int} = -\rho g \sin(\theta) - \frac{f \cdot \dot{m}|\dot{m}|}{4r \cdot A^2 \rho} - \frac{1}{A} \cdot \frac{d}{dz}\left(\dot{m}u\right) \tag{4.14}$$

NB. The factor $\dot{m} \cdot |\dot{m}|$ is included to preserve the sign convention of flow, instead of the $\dot{m}^2$ often present in literature. In this model, $\dot{m}$ is negative, since it travels against the z axis.

Multiple equations exist for the friction coefficient $f$; we will use the Colebrook equation:

$$\frac{1}{\sqrt{f}} - 1.74 + 2 \cdot \log_{10}\left(2 \cdot \epsilon + \frac{18.7}{Re \cdot \sqrt{f}}\right) = 0 \tag{4.15}$$

where $\epsilon$ is the roughness of the pipe (see Table 4.1); and the Reynolds number ($Re$) is defined as:

$$Re = \frac{2 \cdot |\dot{m}|}{\mu \cdot \pi \cdot\ r_w} \tag{4.16}$$

### 4.2.3. Tubing Performance: Two Phase Flow

The equations for two phase flow obey the same physical principles. However, a more complex system of equations with additional parameters is required to describe it.

For two phase flow, mass flow is expressed as the sum of phases:

$$\frac{d}{dz}(\dot{m}_g + \dot{m}_l) = 0 \tag{4.17}$$

We introduce the steam fraction $x$ -also called steam quality in literature. It is the ratio of gaseous to total mass flow rate.

$$x = \frac{\dot{m}_g}{\dot{m}_g + \dot{m}_l} = \frac{\dot{m}_g}{\dot{m}} \tag{4.18}$$

To describe the momentum conservation in two phase flow, three simple additions are necessary to Eq. 4.14: the expression of density as the weighted average of each phase, a two phase multiplier $\Phi^2$ for the frictional term, and the expansion of the inertial term to include both phases.

$$\frac{dp}{dz}_{int} = -((1-\alpha)\rho_l + \alpha\rho_g)\, g \sin(\theta) - \frac{f \cdot \dot{m}|\dot{m}|}{4r \cdot A^2 \rho_l} \cdot \Phi^2 - \frac{1}{A}\frac{d}{dz}\left(\dot{m}_l u_l + \dot{m}_g u_g\right) \tag{4.19}$$

The velocity $u$ of each phase can be expressed similarly to Eq. 4.13.

$$u_l = \frac{\dot{m}_l}{\rho_l A_l} = \frac{(1-x)\dot{m}}{\rho_l \cdot (1-\alpha)A} \tag{4.20}$$

$$u_g = \frac{\dot{m}_g}{\rho_g A_g} = \frac{x\dot{m}}{\rho_g \cdot \alpha A} \tag{4.21}$$

Substituting into the rightmost term of Equation 4.19 gives us:

$$\frac{1}{A}\frac{d}{dz}\left(\dot{m}_l u_l + \dot{m}_g u_g\right) = \frac{1}{A}\frac{d}{dz}\left((1-x)\dot{m} \cdot \frac{(1-x)\dot{m}}{\rho_l \cdot (1-\alpha)A} + x\dot{m} \cdot \frac{x\dot{m}}{\rho_g \cdot \alpha A}\right) = \frac{\dot{m}|\dot{m}|}{A^2} \cdot \frac{d}{dz}\left(\frac{(1-x)^2}{\rho_l \cdot (1-\alpha)} + \frac{x^2}{\rho_g \cdot \alpha}\right) \tag{4.22}$$

Due to the complexity of theoretical modelling of two phase flow, empirical correlations will be considered to define the void fraction $\alpha$ and two phase friction correlation factor $\Phi^2$. Multiple correlations exist, each one obtained under a limited range of conditions. In this study, we will consider the Rouhani-Axelsson (1970) void fraction and Beattie (1973) $\Phi^2$ correlations.

The parameter $\Phi^2$ [−] is defined as the ratio between the frictional pressure gradient caused by two phase flow and liquid only flow with the same flow rate. Beattie [4] proposes a set of empirical correlation (p. 398). Here we will use:

$$\Phi^2 = \left[1 + x \cdot \left(\frac{\rho_l}{\rho_g} - 1\right)\right]^{0.8} \cdot \left[1 + x\left(\frac{(3.5\mu_g + 2\mu_l) \cdot \rho_l}{(\mu_g + \mu_l) \cdot \rho_g} - 1\right)\right]^{0.2} \tag{4.23}$$

In equation 4.19, the void fraction $\alpha$ [−] is the proportion of the vapour phase in terms of cross sectional area. In a no-slip model both phases would be travelling at the same velocity; therefore, the steam quality $x$ and void fraction $\alpha$ would be identical.

$$\alpha = \frac{A_g}{A} \tag{4.24}$$

As outlined in Rouhani and Axelsson [38], $\alpha$ can be calculated empirically as Eq. 4.25 (p. 386). It was chosen because it is able to capture the inversion of the characteristic curve:

$$\alpha = \left[\frac{x}{\rho_g}\right]\left[(1+0.12(1-x)\left(\left(\frac{x}{\rho_g}\right)+\left(\frac{1-x}{\rho_l}\right)\right)+\frac{(1.18(1-x))(g\sigma(\rho_l-\rho_g))^{0.25}}{|\dot{m}|/A\ \rho_l^{0.5}}\right]^{-1} \tag{4.25}$$

### 4.2.4. Boundary Conditions

In this subsection, the boundary conditions and constants of the model will be presented. These were derived from databases and technical reports provided by Orkuveitan, or approximated from the available literature.

For the conservation of momentum and energy equations, a boundary value is required at the first node: the reservoir.

From the given data, the following are obtained for a sample unstable and stable well (NG-07 and NJ-14, respectively): top hole specific enthalpy $h_{tf}$; and reservoir pressure $p_{res}$ and temperature $T_{res}$. These were backed up by Bodvarsson et al. (1988) [6]). The well depth $z$, casing depth $z_{casing}$ and well radius $r$ are taken from the technical reports.

Although fluctuating, well head pressures seem to oscillate around a constant value -for the unstable well (see similar patterns in Fig. 3.2 for a different well). It is to be deduced that this particular $WHP$ corresponds to an (unstable) operating condition of the system. When modelling, we will thus use this value as the constant (pre-instability) well head pressure.

| | |
|---|---|
| $h_{tf}$ | 1260 kJ/kg |
| $p_{res}$ | 160 bar |
| $z$ | 2000 m |
| $z_{casing}$ | 600 m |
| $r$ | 3.5" (0.0889 m) |
| $WHP$ | 20 bar |
| $\dot{m}_{op}$ | 11.7 kg/s |
| $\epsilon$ | 0.045 mm [44] |

**Table 4.1:** Boundary conditions for unstable well (NG-07)

| | |
|---|---|
| $h_{tf}$ | 1242 kJ/kg |
| $p_{res}$ | 82 bar |
| $z$ | 1304 m |
| $r$ | 3.5" (0.0889 m) |
| $WHP$ | 16 bar |
| $\dot{m}_{op}$ | 32.4 kg/s |
| $\epsilon$ | 0.045 mm [44] |

**Table 4.2:** Boundary conditions for stable well (NJ-14)

An evaluation of chemical data from the geothermal fluid shows that it is relatively pure water (ca. 1250 ppm of impurities for liquid, 5000 ppm for vapour), this allows us to use a standardised database to

calculate the properties of the fluid with certain confidence. These include density $\rho$ and viscosity $\mu$ of each phase, and steam fraction $x$.

Here, we used the `iapws.IAPWS97` library, provided by the International Association for the Properties of Steam and Water [46].

Regarding energy conservation, bottom hole and top hole enthalpies will be now compared. The enthalpy at the reservoir is calculated using the given pressure and temperature data; while the value at the well head is given in Table 4.1.

The results (Table 4.3) show a slight decrease in enthalpy along the well (ca. 200 kJ/kg). This phenomenon is observed across all wells. For simplicity, a reversible adiabatic ($\Delta h = 0$ ; $h = h_{tf}$) system was chosen. The implications of this simplification will be discussed further along.

| | |
|---|---|
| $p_{res}$ | 160 bar |
| $T_{res}$ | 325ºC |
| Calculated $h_{res}$ | 1483 kJ/kg |
| Known $h_{tf}$ | 1260 kJ/kg |

**Table 4.3:** Enthalpy calculations for unstable well

### 4.2.5. Numerical Modelling

The modelling will be implemented using an up well Forward Euler scheme in Python with $n$ nodes in the z direction. The system of equations is presented for any $\dot{m}$ in Eq. 4.26.

$$\begin{cases} p_n = BFP \\ p_{k-1} = p_k - \left(\frac{dp}{dz}\right)_k \cdot \Delta z \;\; for \; k \; \epsilon \; [1, \; n] \\ p_0 = THP \end{cases} \tag{4.26}$$

Firstly, the BHP is calculated via the Inflow Performance Relation (Eq. 4.8) for any $\dot{m}$. Then, the pressure at each step $k$ is calculated as the fluid travels up the well bore, until the surface is reached ($k = 0$). The properties of the fluid -namely $x$, $\rho_l$, $\rho_g$, $\mu_l$, $\mu_g$ and $\sigma$- are evaluated at each step $p = p_k$ and the constant enthalpy $h$ using the `IAPWS97` library.

The term $\left(\frac{dp}{dz}\right)_k$ corresponds to Eq. 4.19. It can be proved that for $p_k$ above the bubble point (i.e. $x = 0$) Eq. 4.19 is reduced to Eq. 4.14.

Evaluating the mass flow derivative along the well (Eq. 4.7) will be evaluated for any operating flow rate $\dot{m}_{op}$ using central differences in $\frac{d}{d\dot{m}}$, with $dm = 10^{-2}$ kg/s.

$$\frac{d}{d\dot{m}}\left(-\frac{dp}{dz}\right)_k^{\dot{m}_{op}} = \frac{1}{2\,dm}\left(\frac{dp}{dz}_k^{\dot{m}_{op}+d\dot{m}} - \frac{dp}{dz}_k^{\dot{m}_{op}-d\dot{m}}\right) \tag{4.27}$$

## 4.3. Results

### 4.3.1. Intermediate results

This subsection will present the intermediate results of the numerical model using data from the unstable example well, NG-07. This is done in an effort to describe the internal process of the numerical model and provide context to the desired results.

Figure 4.8 presents the output from Eq. 4.8 as an Inflow Performance Relation (IPR). In it, a linear relation is observed, characteristic of a liquid only regime -where changes in density and viscosity with pressure are negligible. This assumption is valid because the pressure remains above the bubble point for our range of mass flow rates $\dot{m}$.

The negative slope implies a local decrease in reservoir pressure as flow rate is increased. The gradient is inversely proportional to the permeability of the reservoir, since a less permeable (lower productivity) reservoir will cause a larger drop in the local pressure. It should be noted that $p_{wf} = p_{res} = 16$ MPa when the well is closed: $\dot{m} = 0$ kg/s.

Returning to Equation 4.5, the external pressure change $\frac{d\Delta p}{dm}_{ext}$ is, in fact, negative -for a constant $WHP$. Therefore, the step between Eq. 4.5 and Eq. 4.6 is reinforced.

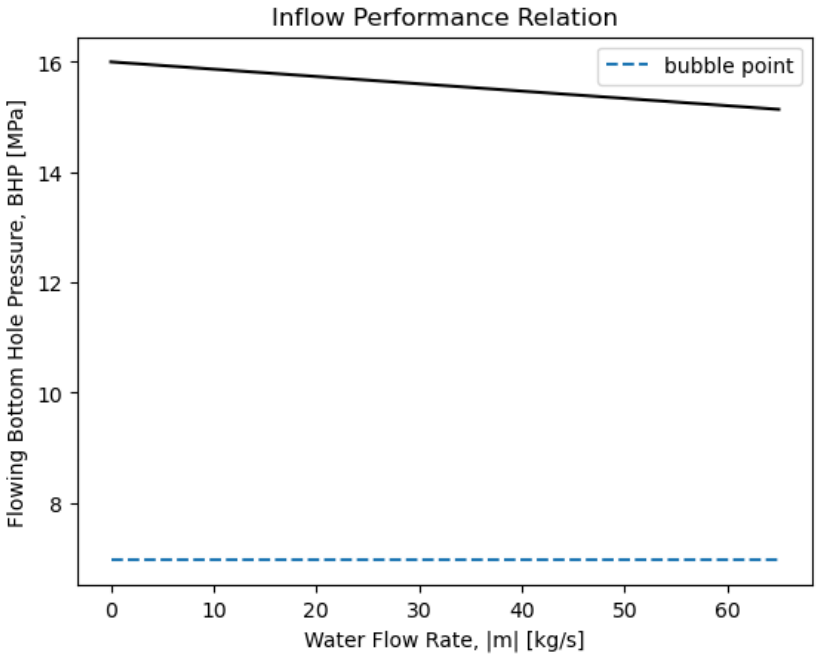


**Figure 4.8:** Inflow Performance Relation

Figure 4.9 plots the pressure along the bore hole for a selection of flow rates using Eq. 4.19. As expected, pressure decreases as the fluid travels upward; however, the magnitude of this internal pressure drop changes significantly with flow rate.

Two regimes can be clearly distinguished: for pressures above the bubble point (6.96 MPa) the pressure gradient is linear -mainly dominated by the constant density of the fluid-, and then becomes non-linear once gas is present in the column.

The different bottom hole pressures correspond to those presented in Figure 4.8 for each flow rate; while the top hole pressures are shown in Figure 4.10.

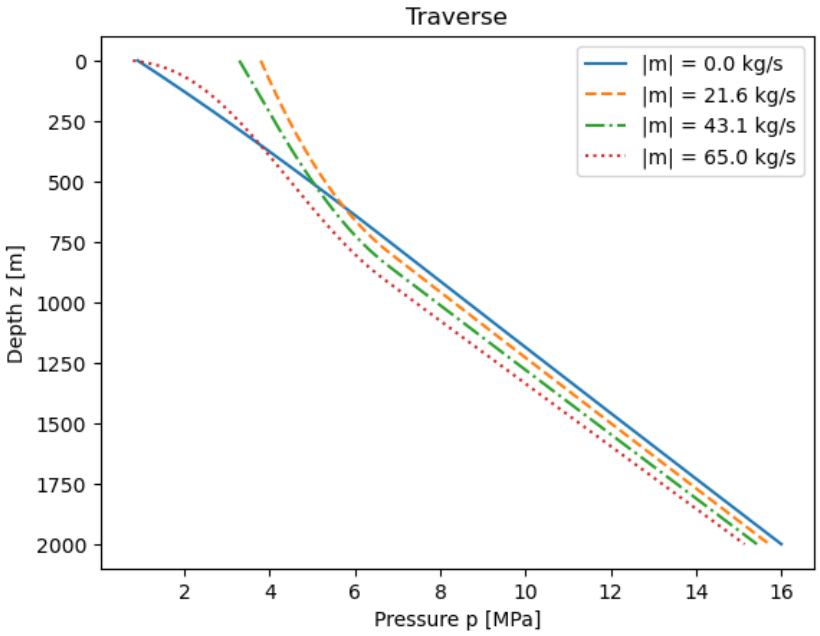


**Figure 4.9:** Well bore traverse

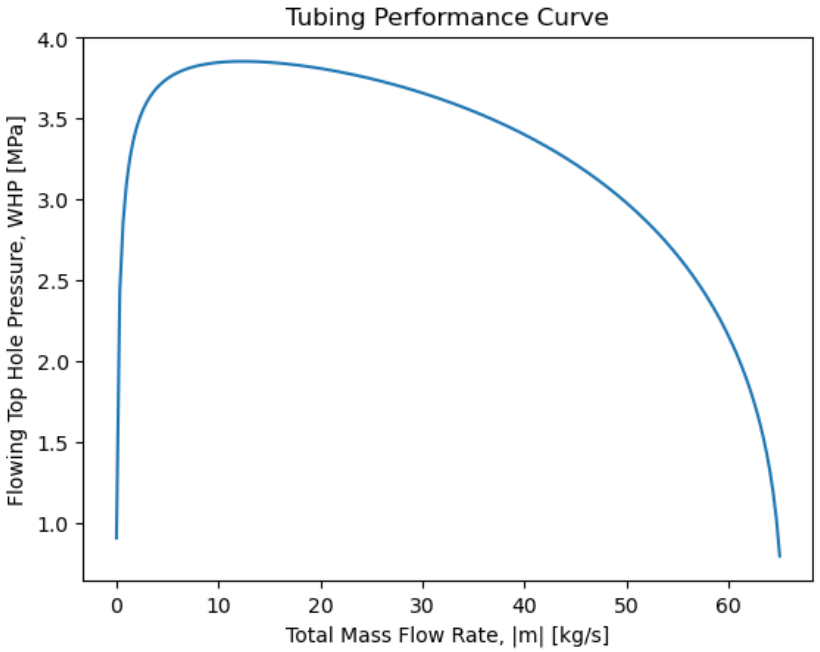


**Figure 4.10:** Well bore Tubing Performance Curve

In figure 4.11, the computed internal pressure $\Delta p$ drop is presented with respect to $\dot{m}$, with each of its components separated. This is done by subtracting the top and bottom hole pressures (i.e. Figures 4.8 and 4.10).

For all flow rates, the greatest change in pressure is caused by gravity loss $\Delta p_{grav}$. Gravity loss is most significant for lower flow rates, causing a phenomenon called liquid hold-up, where the (lighter) vapour is produced and the (denser) liquid is stagnant in an annulus along the tubing. This effect can be clearly seen in Figure 4.9.

Friction and acceleration losses are negligible for reduced flow rates but grow exponentially thereafter, since they both are proportional to $\dot{m}^2$. Furthermore, the two phase friction correction factor $\Phi^2$ grows exponentially at pressures lower than 2 MPa (see Fig. 9.1), causing the friction loss to further increase.

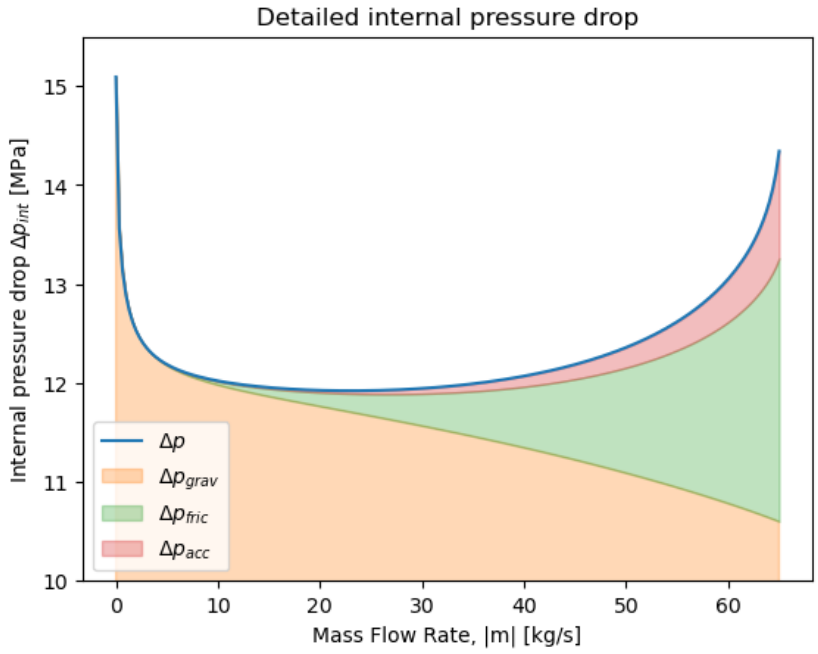


**Figure 4.11:** Internal pressure drop by components (unstable well)

As described previously, the relation between pressure drop $\Delta p$ and mass flow rate $\dot{m}$ is known as the characteristic curve. The derivative of this curve is used to evaluate the Ledinegg stability condition, seen in Equation 4.6. In the next subsection we will analyse these results in detail, and compare the outputs from a stable and an unstable example wells.

### 4.3.2. Characteristic Curves and Along Well Stability

To put this into context, we briefly return to the theoretical background of this chapter.

The Ledinegg stability criterion, expressed in Equation 4.6, states that a certain operating condition will cause instability in the flow if the derivative of the characteristic curve $\frac{d\Delta p_{int}}{d\dot{m}}$ is negative for the mentioned conditions.

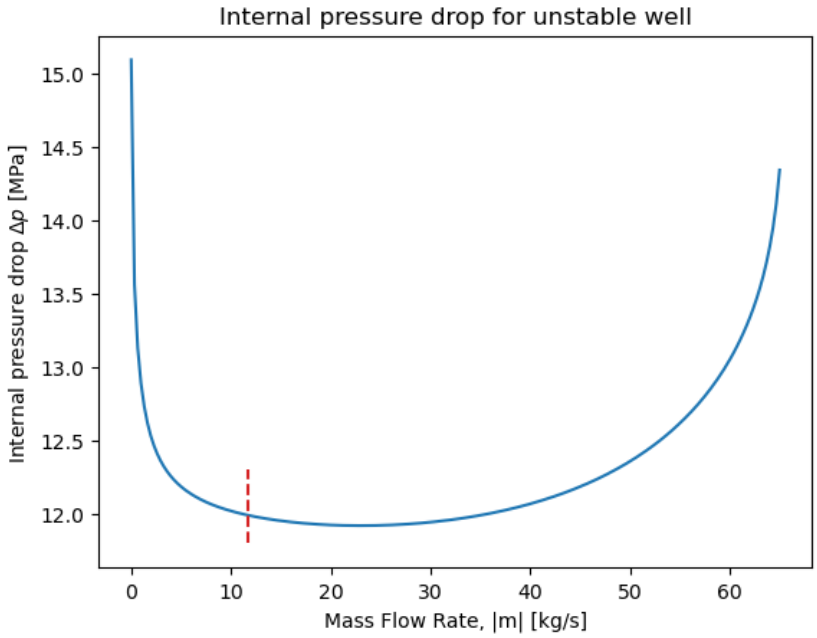


**Figure 4.12:** Characteristic curve for unstable well (NG-07). The well radius is r = 89 mm.

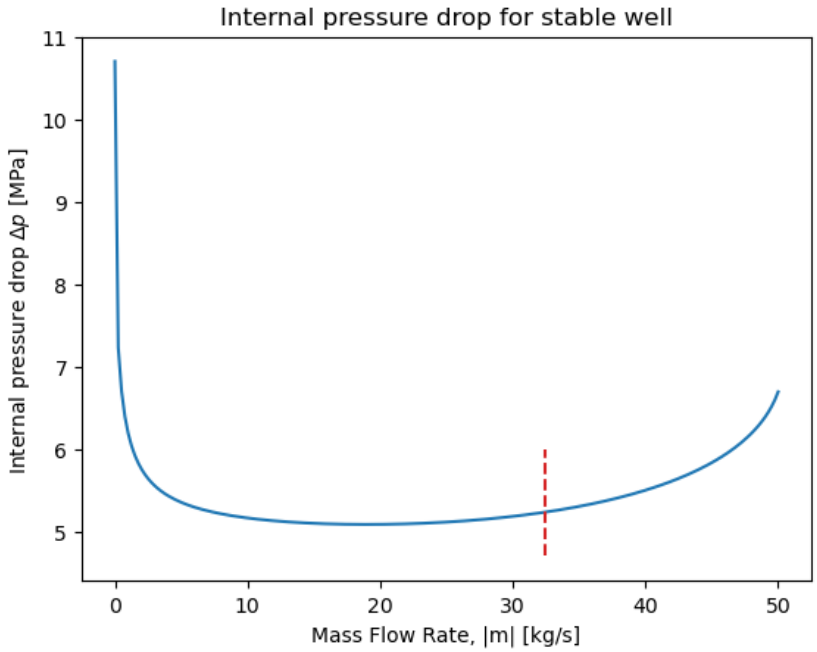


**Figure 4.13:** Characteristic curve for stable well (NJ-14).

Figures 4.12 and 4.13 present the internal pressure drop for the stable well NJ-14 and the unstable well NG-07 with respect to the mass flow rate (i.e., the characteristic curve). The red dashed line shows the operating flow rate, as given in Tables 4.1 and 4.2.

It can be clearly seen that for the functioning well, the operating flow rate is in the stable region ($\frac{d\Delta p_{int}}{d\dot{m}} > 0$), while the fluctuating well operates in the unstable region ($\frac{d\Delta p_{int}}{d\dot{m}} < 0$).

The interpretation of these results appears to indicate that the instability of the wells may be described as a Ledinegg instability. However, the extremely reduced sample size of only two wells cannot provide a rigorous comparison. A more detailed analysis should be done across multiple wells to determine if this hypothesis is valid.

Furthermore, these results are unable to provide a reasoning why the fluctuating well remains in the unstable solution and does not experiment a flow excursion -i.e. the system migrating to a stable point-, as is expected under most conditions (Ruspini et al., 2013, p. 524). The fact that the well stays under unstable conditions implies that the characteristic curve (Fig. 4.12) is being modified as a flow excursion is observed, reevaluating the stability and establishing a cyclical behaviour (as described in Figure 4.6).

Overall, the authors find that there is an indication toward Ledinegg instability being the cause of the observed fluctuations. However, there is a large uncertainty in these results, and further research is needed to validate them.

As for the stability along the well (described in Equations 4.7 and 4.27), the results will be presented for three (hypothetical) operating mass flow rates $\dot{m}_{op}$: 1, 25 and 60 kg/s, for each well.

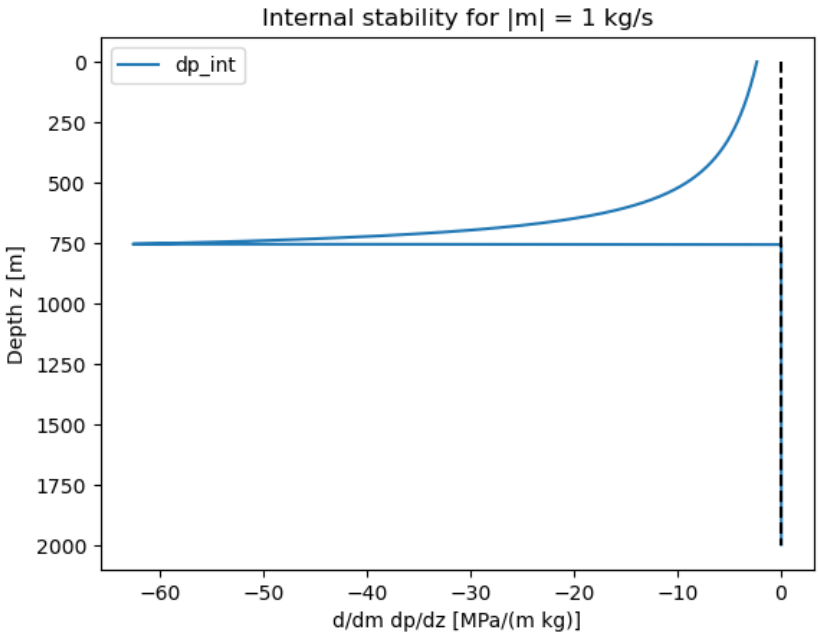


**Figure 4.14:** Internal stability evaluation for unstable well NG-07 (I)

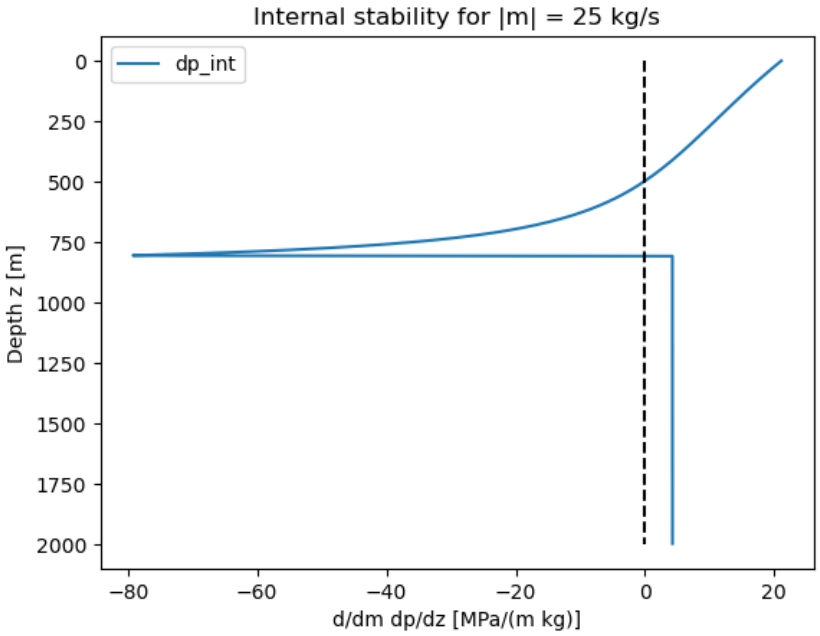


**Figure 4.15:** Internal stability evaluation for unstable well NG-07 (II)

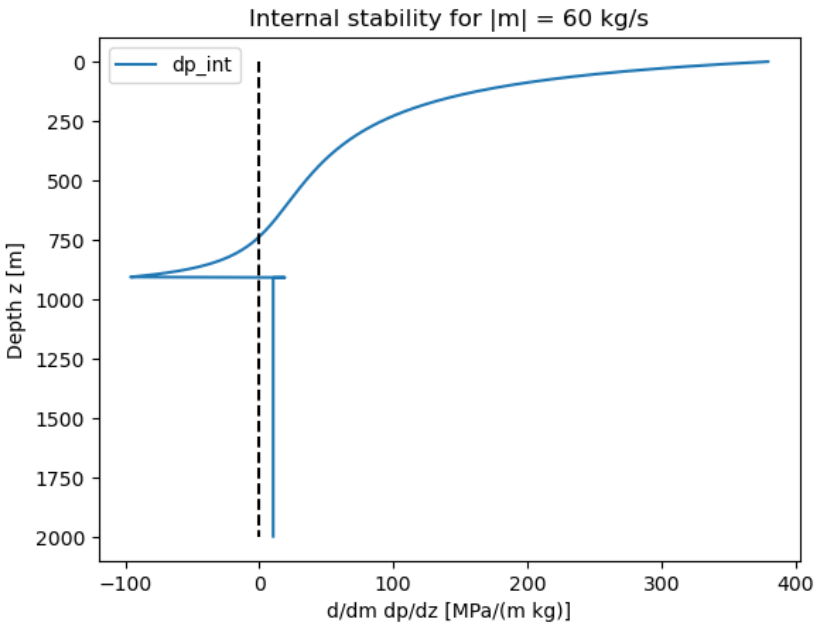


**Figure 4.16:** Internal stability evaluation for unstable well NG-07(III)

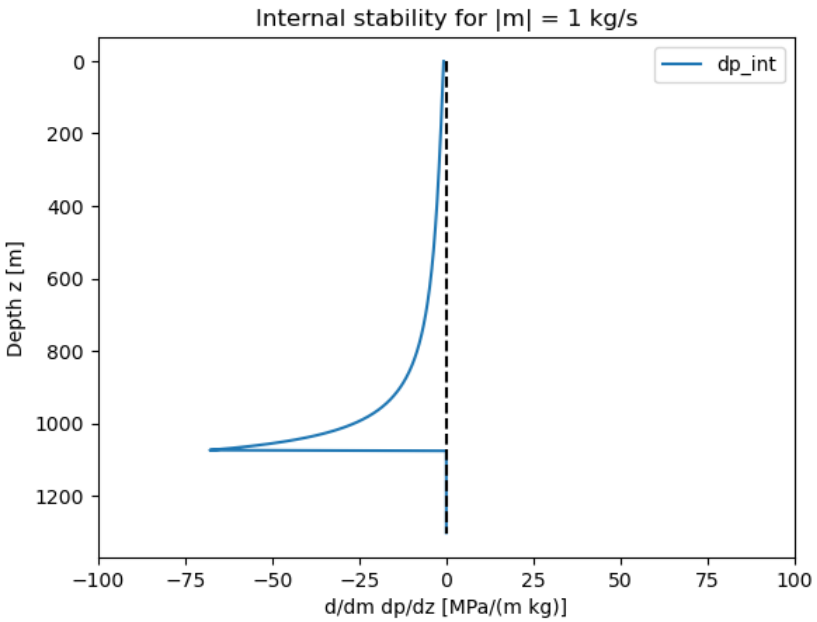


**Figure 4.17:** Internal stability evaluation for stable well NJ-14 (I)

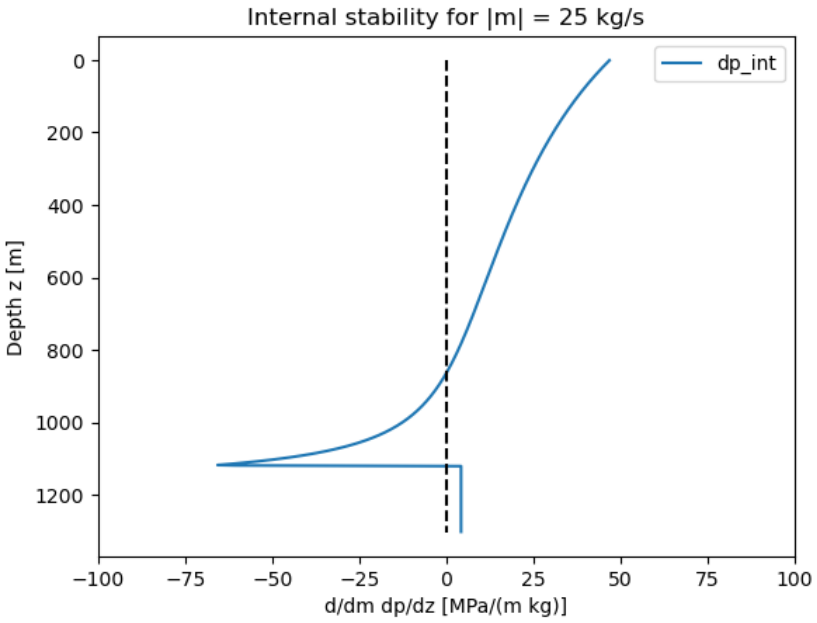


**Figure 4.18:** Internal stability evaluation for stable well NJ-14 (II)

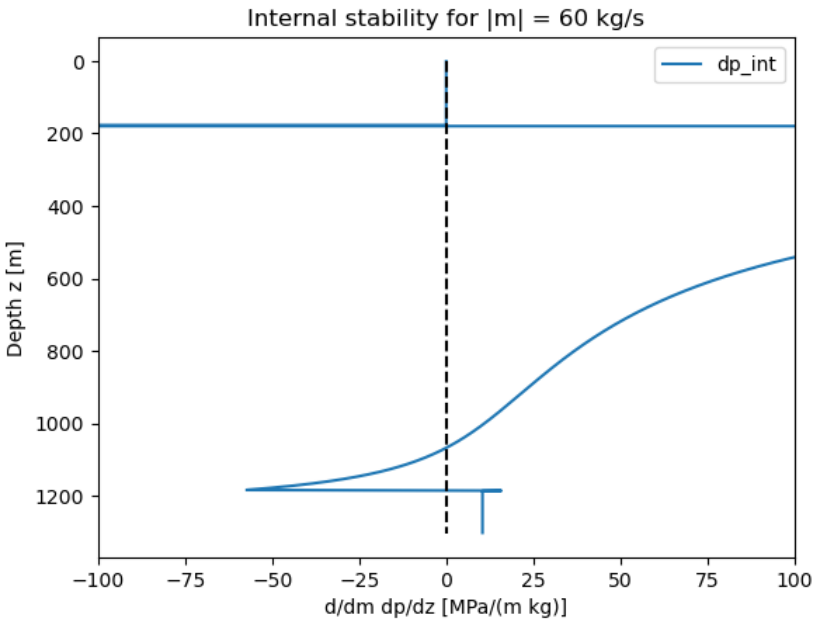


**Figure 4.19:** Internal stability evaluation for stable well NJ-14 (III)

In all cases, the shape of the curve is reminiscent of that presented in the original paper ([41]), with a near-zero positive value until the depth at which the bubble point is reached (see Fig. 4.9), followed by a plunge into negative values (unstable) and a steady increase -in cases returning to positives.

This indicates that, according to our model, both wells have a range of depths at which instability can develop.

The magnitude and depth range of the negative spike is dependent on the mass flow rate. For smaller flow rates, the value of $d/dm\ dp/dz$ does not decrease significantly, but the length of the unstable region is at its largest. The opposite effect is true for higher flow rates. Note that the horizontal line at ca. 200 m in Figure 4.19 is a numerical artifact of pressure reaching atmospheric conditions.

The interpretation of these results is complicated by the abstract nature of the stability parameter $(\frac{d}{d\dot{m}}(\frac{dp}{dp}))$.

Figures 4.14, 4.15 and 4.16 can be compared between each other, and so can 6.1, 4.18 and 4.19; but the physical implications of these results are unknown beyond a stable/unstable dichotomy.

The results indicate both wells present, for any flow rate, a range of depths where instabilities may develop; therefore, both wells should be unstable to an unknown degree. According to Shulyupin [41], 'these characteristics are common to all steam-water wells. ... Pressure fluctuations are considered to be a natural property of steam-water well. These fluctuations [under condition 4.7] usually are not an obstacle for its practical use. Therefore, in practice, a sufficient condition for stability can be considered [Eq. 4.6].' (p. 294)

The fluctuations caused under condition 4.7 presented in the aforementioned paper (see Figure 4.20) occur on average 3 times per day, and have an amplitude no larger than 0.2 bars -as opposed to the ca. 9 days and 5-10 bars of amplitude observed in the studied wells.

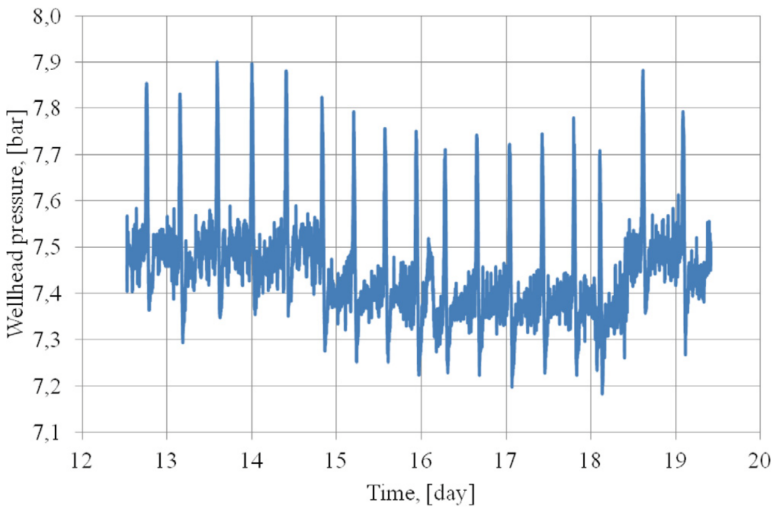


**Figure 4.20:** Wellhead pressure fluctuations from Shulyupin [41]

The authors find that the fluctuations produced under instability condition 4.7 are most likely not responsible for the periodic oscillations observed in the Hengil wells studied. Since, according to sources, these fluctuations are present in all wells and are often not noticeable.

Therefore, the conclusion of the Internal Flow Instability hypothesis is that Ledinegg Instability under Equation 4.6 may be a cause for the studied fluctuations. However, more research is required to validate this hypothesis. Equation 4.7 cannot thus be used to assess the origin of the observed fluctuations.

# 5 Multiple Feed Zones theory

This chapter expands on the Multiple Feed Zones theory, based on the work of Yamamura et al. [48] and Matsumoto et al.[29]. Section 5.1 explains the theory behind the hypothesis, Section 5.2 describes the methods used to test the hypothesis which is then split into two sections: Section 5.3 on modelling with CMG software and Section 5.4 on simulations with the model from the Japanese research team.

## 5.1. Literature

The Multiple Feed Zones Theory is based on a series of papers by a team of Japanese researchers from high-enthalpy geothermal wells in Japan, which showed oscillations in pressure and flow rates [48]. According to their findings, the oscillations in well head pressure in these wells are caused by the interaction of two feed zones at different settings of temperature and pressure. Yamamura et al. [48] have developed a numerical model to test their theory. A simplified version of the process model is illustrated in Figure 5.1.

During the process, single phase water continuously flows into the well from the deepest feed zone and continues flowing upward. Due to the lower pressure inside the well, the hot liquid partially vaporises, resulting in a two-phase flow that continues to travel towards the well head. Further up the well, more liquid water enters the well from the second shallower feed zone, forming an accumulation of single phase water on top of the approaching two-phase column. As this single phase water ascends in the well bore, its pressure decreases, and the single phase column suddenly begins to vaporise and also transforms into a two phase column, causing an explosive discharge. The sudden pressure drop allows new inflow from the shallow feed zone, building up the single phase column on top of the two phase column again and repeating the process.

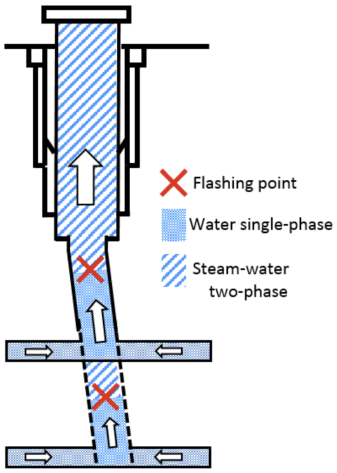


**Figure 5.1:** Schematic drawing of single and two phase flow in a well bore with two feed zones. [48].

Figure 5.2 shows the physics behind the cycles of single phase fluid build-up on the left. The fluid entering from the deep feed zone is hotter and has a higher specific enthalpy [48]. Firstly, due to an increase in pressure in the upper feed zone, the mass flow rate of this feed zone is reduced, preventing

the liquid from entering the well. This also reduces the ratio of the mass flow rate from the shallow feed zone in terms of the total flow rate in the well ($R_s$) [48]. As more of the higher enthalpy fluid from the deep reservoir flows through the well bore, the specific enthalpy ($h_{mix}$) of the fluid in the well (from both feed zones combined) increases at the outlet point of the upper feed zone. This leads to a decrease in the pressure difference between the wellhead and the upper feed zone ($\Delta P^{wh}_{fzs}$) and a decrease in the average density ($\rho_{aves}$). The density decrease induces a pressure drop in the shallow feed zone ($P_{fzs}$), which in turn generates a higher mass inflow rate from the shallow feed zone, simultaneously increasing $R_s$ and decreasing $h_{mix}$. While the low-enthalpy fluid from the shallow feed zone moves further up through the well bore, the average density increases, as does the pressure difference between the wellhead and the shallow feed zone, which leads to the pressure in the shallow feed zone increasing again and the cycle repeats. In the Japanese study described above [48], production eventually ceases when the high enthalpy fluid from the deep feed zone reaches the shallow feed zone. The corresponding simulated density and specific enthalpy cycles are shown on the right side of the Figure 5.2.

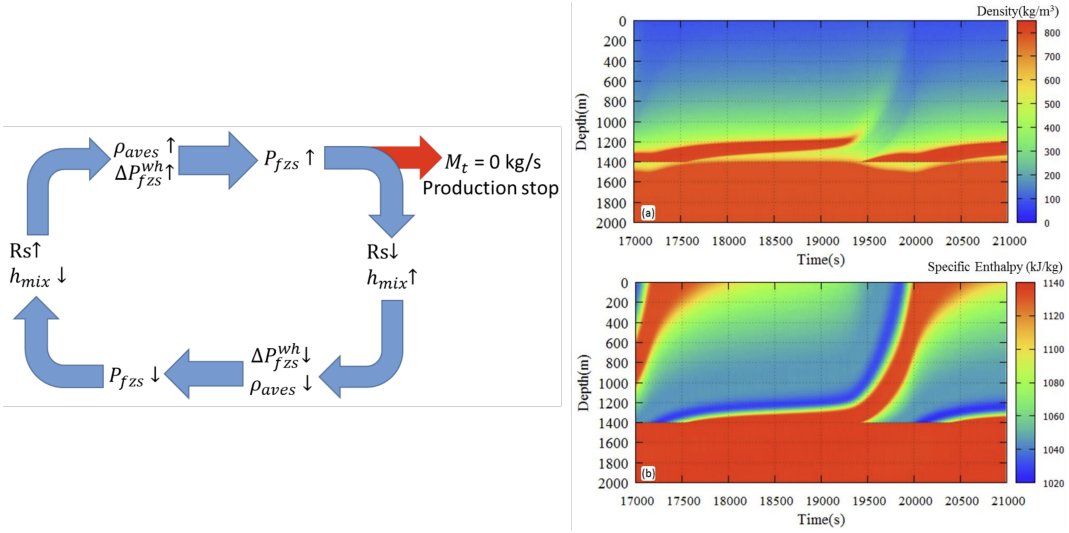


**Figure 5.2:** Mechanism causing pressure oscillations on the left, density and specific enthalpy in the well bore on the right. [48].

Given that the wells at Reykjanes are drilled into a fractured basalt reservoir and all the wells under investigation are reported to have more than 5 feed zones, the phenomenon of interaction between the multiple feed zones with different enthalpies is considered and researched. The reservoir depths are the same for both Japanese and Icelandic wells, although the locations and depth of the feed zones differ. Furthermore, the wells studied in this paper are substantially hotter, with 325 °C in the bottom feed zone at 2000 m for well NG-07, compared to the 260 °C used in the simulation of Matsumoto et al. (2021) [29]. The higher temperature is accompanied by higher pressures, with well NG-07 reaching approximately 150 bar at 2000 m, compared to 100 bar at the same depth in their model.

Although data on the flow rates of the Icelandic wells is not measured continuously, the fluctuations in wellhead pressure are comparable to the simulation output of Matsumoto, Itoi, and Fujimitsu [29] as can be seen in Figure 5.3. The amplitudes of the fluctuations in the wellhead pressure are slightly smaller in the case of the Japanese wells, although comparable to well NG-07. For two shallow feed zone temperature estimates, the results of the temperature simulation are shown in Figure 5.3. The pressure fluctuations reach close to 10 bars, whilst they can reach up to 15 bars for NG-07, and 20 bars

for well NJ-15 as shown above in Figure 2.6. The frequency of pressure and production rate reported in Figure 5.3 are nearly identical, so comparisons between the flow rate frequency of these simulation results and the pressure oscillations retrieved from the data on the Icelandic wells will be made.

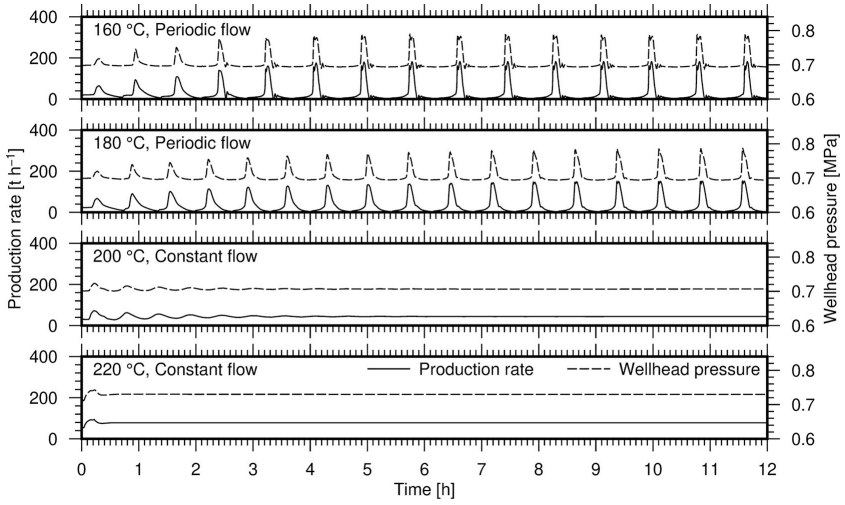


**Figure 5.3:** Production rates and wellhead pressures for different shallow feed zone temperatures against time. [29].

The model of Matsumoto et al. [29] is based on their previous model from 2017, published by Yamamura et al. [48]. The initial model was improved by adopting a fully implicit time integration to improve numerical stability. Matsumoto et al.[29] assumed a temperature of 260 °C in the deep feed zone at a depth of 2000 metres and varied the temperature of the shallow feed zone at 1400 m depth between 180-240 °C. Depending on the temperature of the shallow feed zone, the flow rates can be stable or fluctuating, as shown in Figure 5.4. Distinctive periodic oscillations occur for temperatures of 180 °C, 200 °C, and 220 °C, whereas stable production rates occur when the temperature in the shallow feed zone is at 240 °C, which is closer to the temperature of the deep feed zone.

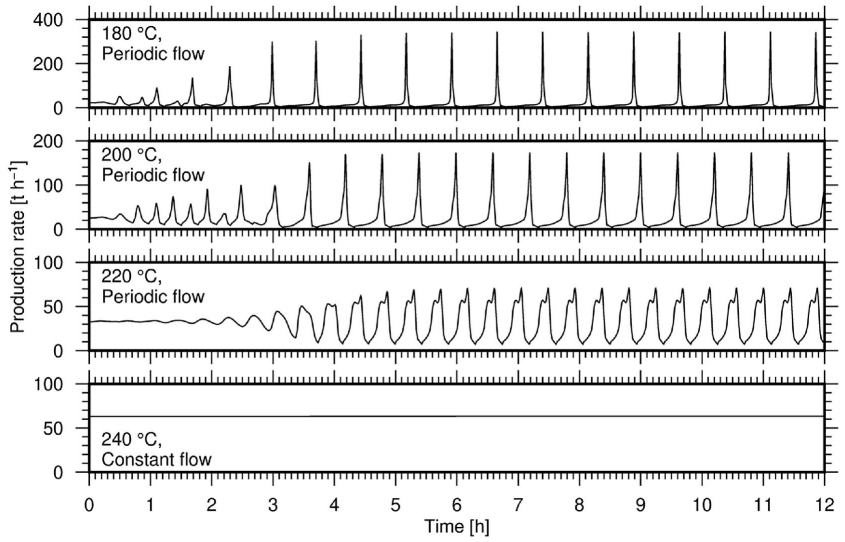


**Figure 5.4:** Production rates for different shallow feed zone temperatures against time. [29].

In addition to the production rate at the wellhead, the model also simulates the inflow from the two

different feed zones over time, as shown in Figure 5.5. The amplitude of the oscillation in the inflow rate in the shallow feed zone is much higher than that of the deep feed zone. This supports the theory that inflow from the shallow feed zone is periodic, decreasing when the single phase column has formed and increasing after an eruption.

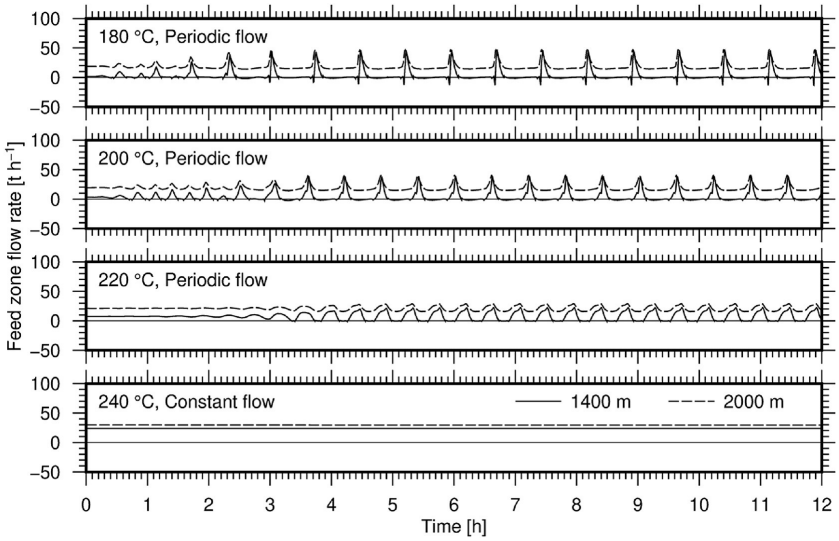


**Figure 5.5:** Inflow rate from the deep and shallow feed zone against time for different shallow feed zone temperatures. [29].

The initial models used in this study assume a constant wellhead pressure boundary condition to perform the simulation. This model was improved by adding a 2000 metre long pipe attached to the wellhead (see Figure 5.6), which allows the calculation of oscillations in wellhead pressure and in outflow rates (see Figure 5.3).

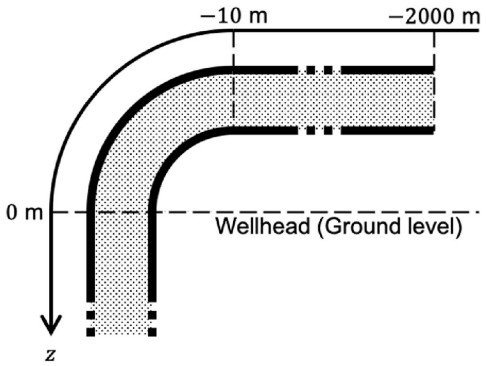


**Figure 5.6:** Schematic of the extended model ([29]

## 5.2. Methodology

To test whether the Multiple Feed Zones theory is applicable to our fluctuating wells, it is required to model two-phase flow in the well bore. We are aiming to simulate the development of two-phase flow in time and space along the well. According to Matsumoto, Itoi, and Fujimitsu [29], instabilities occur in the flow rate and well head pressure if two phase fluid is trapped underneath single-phase feed zones of lower enthalpy. Meeting this exact condition is the main goal of the simulation in CMG STARS.

Furthermore, transient pressure and flow rate can be modelled to determine if they exhibit instabilities. The specifications of this model are explained in detail in section 5.3.

To confirm the results from STARS, the model developed by Matsumoto et al. [29] was used to simulate fluctuations in the outflow rate using his mixed-phase enthalpy conservation model with no-slip between the phases (homogeneous flow model). The aim of the simulation was to reproduce conditions similar to those in well NG-07 in order to test whether pressure fluctuations could come from the mixing of fluids with different enthalpies. The intention was not to replicate the exact pressure-fluctuation behaviour of well NG-07, but to verify that the physics of this theory can cause fluctuations in this well.

## 5.3. Modelling with STARS

STARS and BUILDER by CMG were used to simulate two-phase flow in well NG-07. The reservoir and well bore models are described in Section 5.3.1, the results in Section 5.3.2, followed by a sensitivity analysis in Section 5.3.3. Remediation measures are explained in Section 5.3.4. Lastly, model limitations are further explained in Section 5.3.5.

### 5.3.1. BUILDER and STARS model parameters

We used CMG BUILDER and STARS to simulate the flow in well NG-07, one of the vertical wells. The model assumes a reservoir volume of 3 km by 3 km and a depth of 2 km. To prevent heat loss from the well into the surrounding rock through the casing during the simulation, only the bottom 1400 m of the reservoir was modelled, as the top 600 m of the well are covered by the casing. The size of the grid cells within the model was chosen as 60 m by 60 m by 10 m, resulting in 50 blocks in both x and y directions and 140 blocks in the z direction. The porosity was set at 0.4 throughout the reservoir and the permeability was set at 1 mD [14]. The volume of the grid cells at the edges of the reservoir was multiplied by 1000 to eliminate the effects on fluid flow caused by the edge of the reservoir model. Initially, the model contained vertical layers of 100 metres, but due to the low granularity of the results, the number of grid cells was increased by 10 times. The grid was not refined further due to the increasing modelling time.

Once the reservoir block model was created, we added the feed zones. These were realised by increasing the permeability in selected horizontal layers. The feed zones were set at depths of 800 m, 1000 m, 1500 m, and 2000 m, which correspond to the actual locations of the feed zones taken from the data set for well NG-07. The feed zone at 1500 m depth is the largest and therefore has the highest permeability of 300 mD in the model, the others are smaller and have a set permeability of 152 mD [37]. An overview of the block model alongside the feed zones is shown in Figure 5.7.

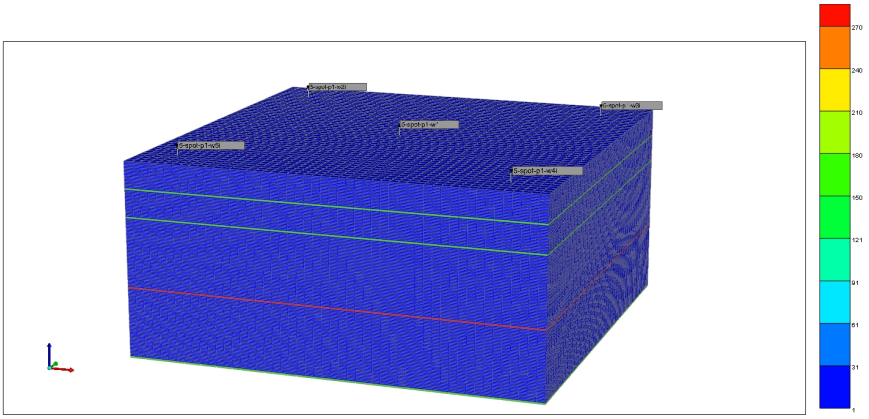

**Figure 5.7:** Overview of the CMG STARS block model while plotting permeability in the x-y directions

The temperature at the bottom of the reservoir is 300 °C. At the bottom of the casing, at 600 m depth, the temperature is 205 °C, according to the PT data of well NG-07. We used a linear interpolation for the temperature gradient between these two known temperature values. The temperature of the bottom feed zone was set at 325°C according to the PT data. The rock conductivity is set to 181440 $J/(m \cdot day\,°C)$ and the heat capacity to $3 \cdot 10^6$ J/(m$^3$ °C) [14].

The initial conditions are the reference pressure, which is set at 60 bar-g at 600 m depth and the water-oil and gas-oil contacts, which are set to 600 m depth. These are set equal because our reservoir does not contain any oil. The simulation starts on the first of January 2000 and runs for 7-10 months, depending on the step size of the models (hours, days or months). By the end of the simulations, the water rate and well head pressure have stabilised.

In our block reservoir model, we added five wells, one production well in the middle and four injector wells, one in each corner with the same distance to the production well. All wells have a borehole model and are of the same size as the production well NG-07. Appendix A provides an overview of the well parameters. The four injector wells inject water at 60 °C at 50 bar-g into all four feed zones, injecting 1.5 km from the producer well. This corresponds to an estimated temperature of the injected water in the Icelandic geothermal field. Cold water does not reach the production well by the end date of our simulation, which means that the injected fluid does not decrease the temperature of the water produced nor the reservoir. The main objective of these simulations is to replicate processes in the producing well. The injectors are added to prevent the system from running dry.

The production well is perforated all the way down from the bottom of the casing, as is the case for well NG-07. To replicate the behaviour of well NG-07 in terms of wellhead pressure and flow rate, the following constraints were set:

- Injector wells are shut-in when the reservoir pressure reaches 50 bar-g which is equal to saturation pressure
- Maximum injection rates per well are 10000 $m^3/day$ to replicate the production rate around 30000 $m^3/day$
- The producer well has a set minimum bottom hole pressure of 10 bar-g. If the BHP is drops below 10 bar-g, then the simulation will set it equal to the limit value.

During simulations, the pressure constraint was met, leading to the injector wells being shut-in. This prevented the pressures in the well from reaching extreme values which could lead to possible fracturing, or would allow too much water in the reservoir.

### 5.3.2. Results from STARS

After running the model described in section 5.3.1, water saturation in depth was plotted for 6 different time steps. The results can be seen below.

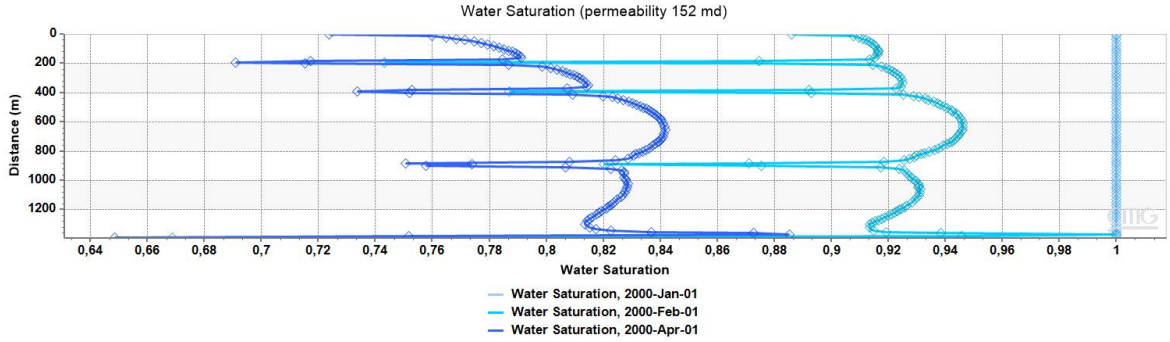


**Figure 5.8:** Water saturation profiles between January and April using the standard model

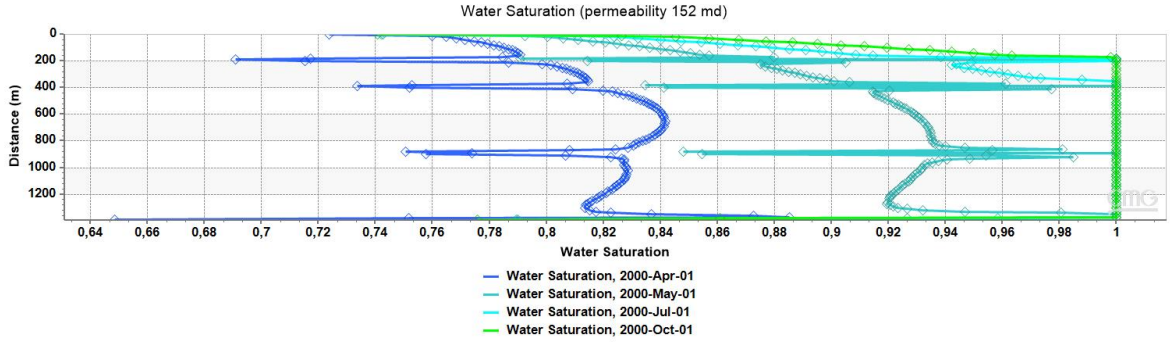


**Figure 5.9:** Water saturation profiles between April and October using the standard model

The water saturation profiles in the well appear to follow a behaviour that can be separated in two stages, as shown, respectively, in Figures 5.8 and 5.9. Initially, the reservoir is saturated with water, as can be seen in the first time step in Figure 5.8. During continued production, the pressure drops, inducing a phase change from water to steam in the well. The amount of steam in the well increases from February to April. This increase occurs throughout the well, although the effect is most striking in the feed zones.

From April on, this trend of decreasing water saturation reverses; see Figure 5.9. First, the feed zones and the cells directly adjacent to them exhibit an increase in water saturation. The water saturation in the feed zones starts to alternate between values 0.85 and 1 at 900 m in May. This phenomenon occurs in every feed zone. However, a general increase in water saturation occurs between May and October, ending with a completely saturated reservoir apart from two phase flow in the upper 200 metres and at the very bottom of the well.

The shift from a general decrease to an increase in water saturation occurs between April and May. This coincides with the start of the fluctuations in the liquid rate, although a specific start date is not visible in Figure 5.10 due to the time step used. This indicates that a two-phase flow beneath a water inflow zone could cause disruptions in the overall flow rate. Following the time step of October in the simulation, the water saturation graph does not change with time any longer, although the liquid rate continues to oscillate.

Furthermore, we decided to plot the liquid rate and pressure in feed zones as a function of time.

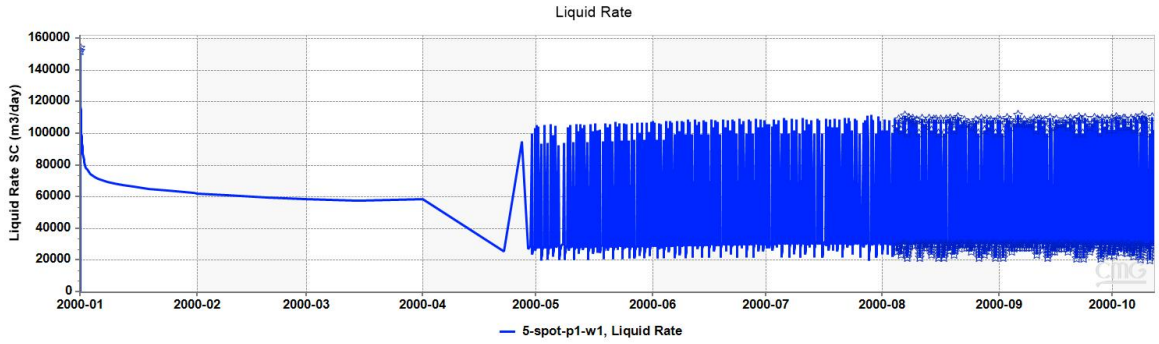


**Figure 5.10:** Liquid rate in the production well

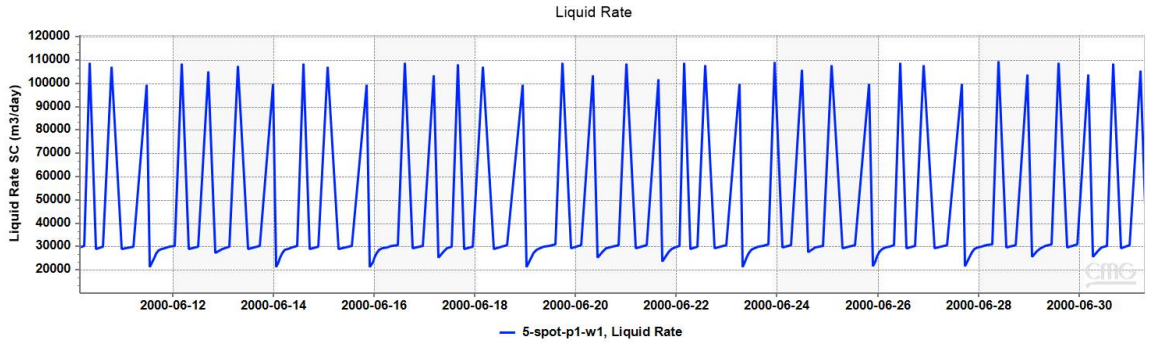


**Figure 5.11:** Zoomed in liquid rate

Here, it can be seen that the well starts fluctuating around late April and has a similar amplitude until the end of the simulation. The period of the fluctuations is approximately 1 day, which is more frequent than in well NG-07, where the period is 6-9 days. The average flow rate is 60 000 $m^3$/day which is 3 times higher than the flow rate in well NG-07.

From August onwards, star-like symbols appear at the peaks of each fluctuation, representing error symbols. Error messages were present throughout the oscillating data; however, they were deleted before August due to plotting errors using CMG RESULTS once the result file was reloaded. These indicate that there are numerical errors and that the pressure values did not converge. The model then sets the reference pressure to the bottom hole pressure, which is part of the boundary conditions. This issue is explained in more detail in Section 5.3.5.

We also plotted pressure profiles in time for the feed zones and at the wellhead.

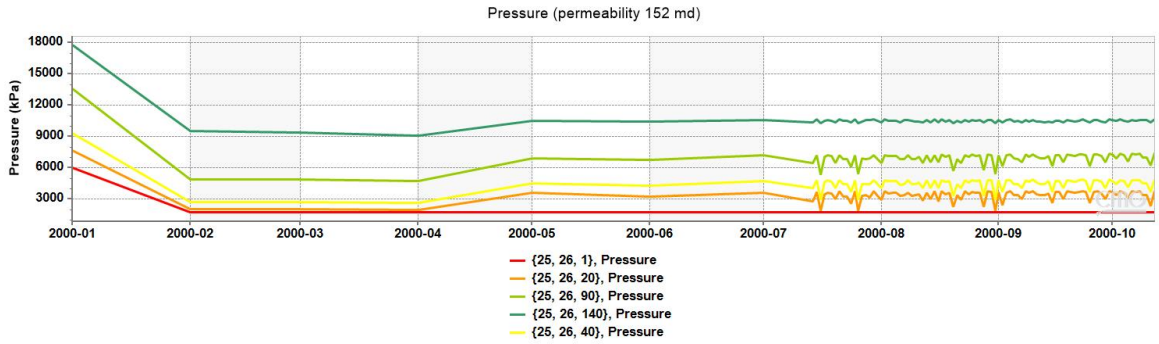


**Figure 5.12:** Pressure in feed zones and at well head

The figure above shows pressure fluctuations in the feed zones, but a stable pressure of 17.4 bar-g at the well head. In this simulation, we know that the fluctuations started in April, but due to the limited storage space available, we simulated the pressure with a time step once a month until mid July and after that with a time step once a day. That is why pressure fluctuations occur later than flow rate fluctuations. Interestingly, these numerical errors did not occur while plotting the pressure profiles.

The figure shows that the higher feed zones show stronger fluctuations than the deeper ones, but we lack real life data to compare these values to. In NG-07 the wellhead pressure fluctuates with an amplitude of around 10 bars, but in the simulation results the wellhead pressure does not fluctuate at all. It is unknown whether pressure fluctuations in the feed zones are affected by the numerical errors that occur when we calculate the flow rate in the well.

### 5.3.3. Sensitivity analysis for STARS

After being able to replicate fluctuations in our simulated well bore, we were interested in investigating the impact of permeability on the model. The objective here was to find out how increasing and decreasing permeability affects the two phase flow and fluctuating behaviour of the simulated well.

First, the effect of lower permeability was tested by changing the value from 152 md to 15 md. This caused several problems and the simulation was not able to run. Setting very low permeability layers produced the following errors:

- Well bore pressure is below Min. pressure value
- Friction pressure drop is high due to high rates or small well radius, causing numerical difficulties.

The next step was to increase the permeability by 10 times from 152 md to 1520 md in the feed zones. The results can be seen below.

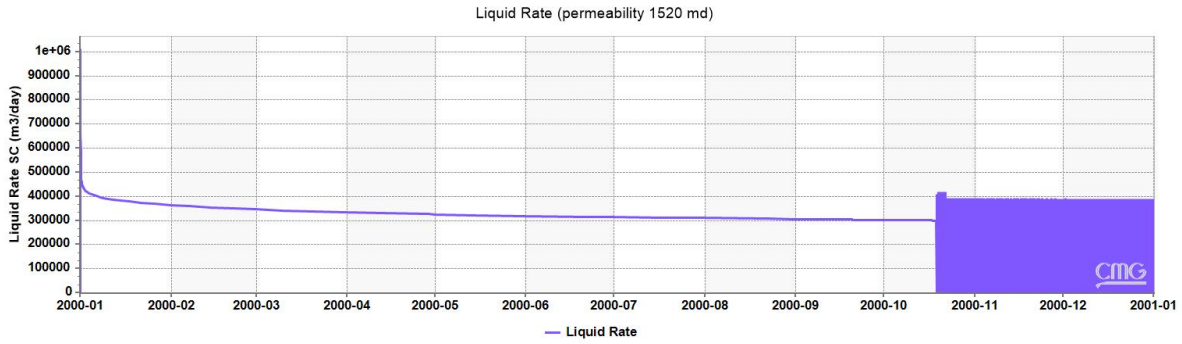


**Figure 5.13:** Liquid rate with increased permeability

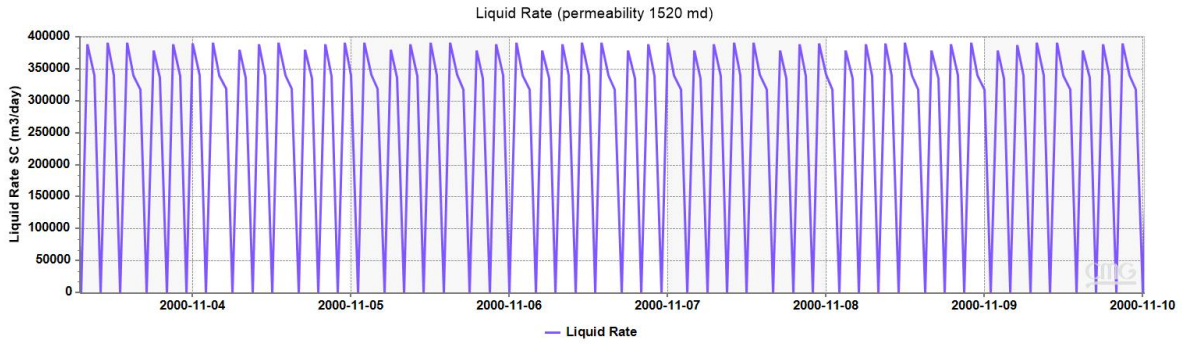


**Figure 5.14:** Zoomed in liquid rate with increased permeability

In this scenario, the liquid rate started to fluctuate on October 18th. The liquid rate oscillated between 0 and 400 000 $m^3$/day, which is a very wide range and the highest value is 20 times larger than the flow rate in well NG-07. In Figure 5.14 it can be seen that the flow rate fluctuates faster in this case - 7 times a day compared to once a day with lower permeability.

Pressure time series was also plotted for each feed zone and wellhead and the results can be seen below.

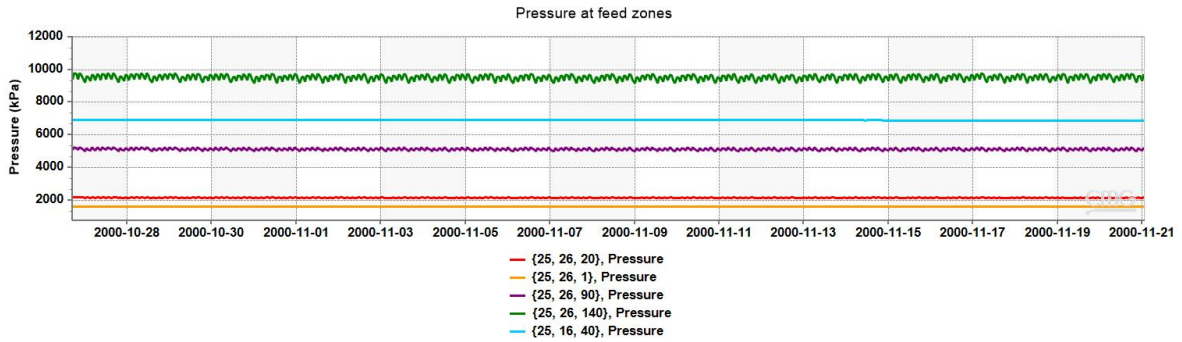


**Figure 5.15:** Pressure fluctuations in feed zones

Figure 5.15 shows that a higher permeability causes the pressure in the deeper feed zones to fluctuate with a higher amplitude than in the shallower inflow zones. This is exactly the opposite of what

happened in the case with lower permeability in Figure 5.12. Furthermore, the feed zone at 1000 m does not fluctuate at all while feed zones below and above are. Like in our previous results, wellhead pressure does not show any fluctuating behaviour.

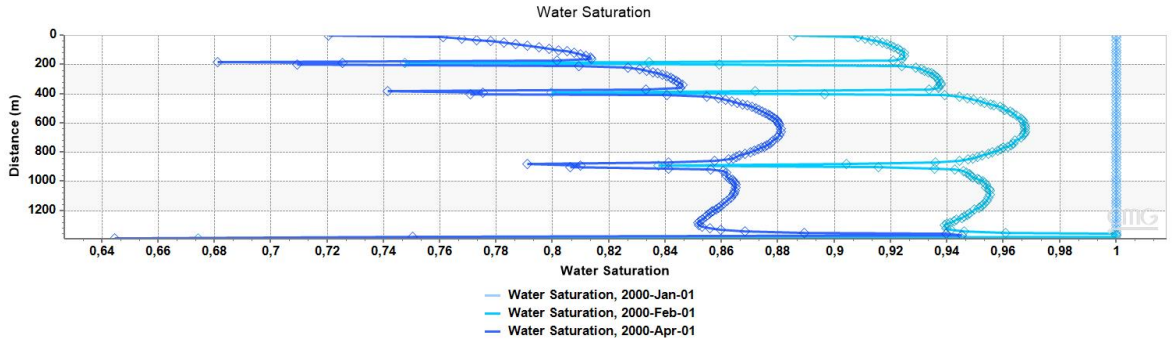


**Figure 5.16:** Water saturation profile between January and April

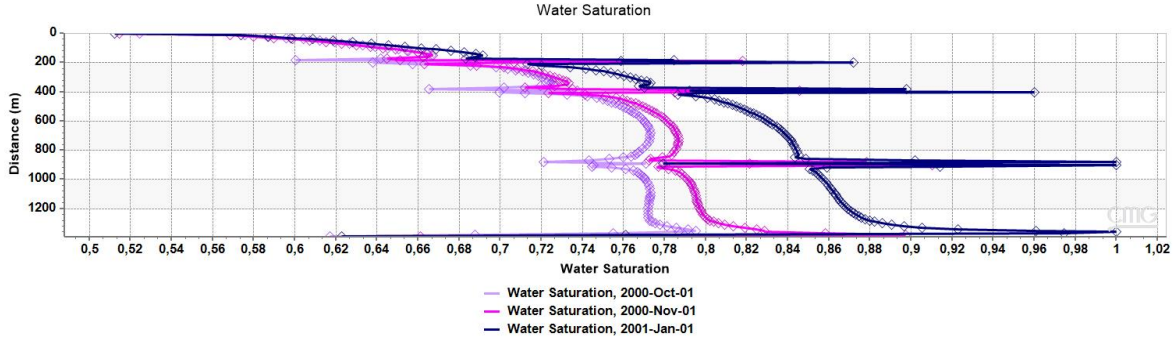


**Figure 5.17:** Water saturation profile between October and January

The water saturation profiles look similar to the previous results. Here, the first stage of increasing the steam content in time is shown in Figure 5.16. The switch to the second stage can be seen in Figure 5.17, where the two-phase fluid is trapped underneath three feed zones with single-phase water inflow. In this graph the simulation does not reach the point where the well is full of one phase water below the shallowest feed zone within the simulated time frame.

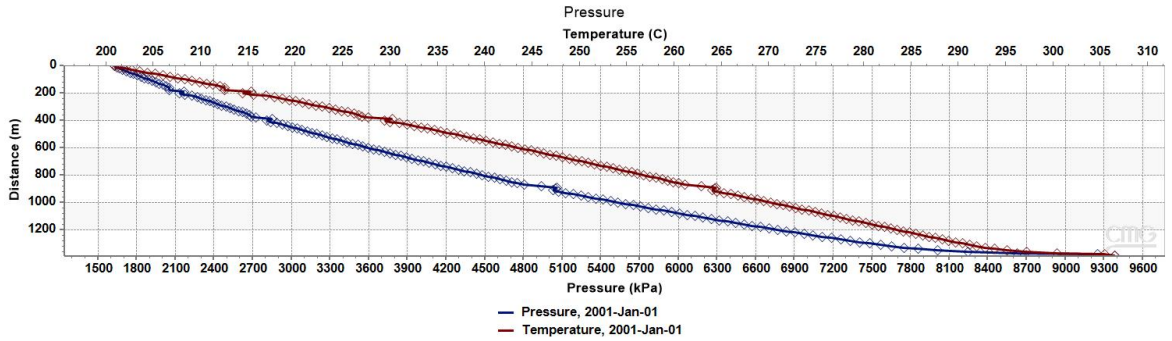


**Figure 5.18:** Pressure and temperature profile with high permeability

Figure 5.18 shows the pressure and temperature profile outputs of STARS using higher permeability in

the reservoir model at the last time step. The temperature profile follows a linear gradient corresponding to the initial condition set, whilst the pressure gradient along the well becomes slightly more parabolic. However, we can see that the four feed zones have an impact on both the pressure and temperature profiles, as they appear to cause minor peaks at the feed zones and at the layers directly adjacent to them. After these regions, the pressure and temperature revert to following their initial gradients.

### 5.3.4. Remediation measures

Oscillating pressure in geothermal wells affects the productivity of geothermal power plants, asking for mitigation measures to stabilise the flow rate. In this chapter, we investigate whether external factors such as lowering the water table and changing the diameter of the well could help manage unwanted pressure fluctuations. These parameters were chosen because they can be easily adjusted, unlike geological factors such as the temperature gradient, porosity, or salinity of the water.

#### Borehole size

First, the simulations were performed with different borehole diameters. We chose two borehole sizes given in CMG BUILDER which were with tubing outer diameter 2 7/8" and 4 1/2". These were the smallest and largest geometries accessible. The details of these sizes are listed in Appendix A.

The results showed that the fluctuating behaviour was still present in both cases and surprisingly the amplitudes and frequencies were identical to our original results. The only difference was that a larger diameter caused the shift in water saturation profiles from the first stage to the second stage to appear one month earlier, in April instead of May.

#### Water-steam contact depth

Secondly, we investigated whether changing the height of the initial steam-water contact could limit the fluctuations. In the initial model, the steam-water contact was set to 600 m which also corresponds to the top of the reservoir and bottom of the casing. It was not possible to increase the water level due to the boundaries of the reservoir. However, lowering the steam-water contact was possible. We experimented with setting the ground water level at 700 m and 800 m depth, and the fluctuations disappeared in both cases. Furthermore, there was no two-phase flow in the well apart from the deepest feed zone and above the steam-water contact (see Figure 5.19) . In the deepest feed zone, the water saturation gradually decreased in time from 1 to 0.75 at the end of the simulation.

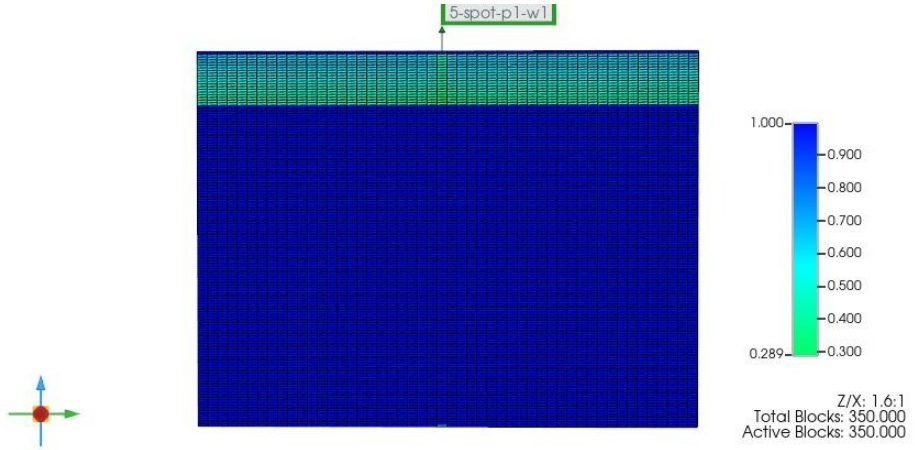


**Figure 5.19:** Water saturation cross profile

Figure 5.19 shows that all the vapour is concentrated above the initial steam-water contact level and the well is almost completely saturated. The fluctuations likely stopped because there is no two phase flow underneath the feed zones.

### 5.3.5. Limitations of STARS

The model had several shortcomings and could not replicate all of the features of well NG-07. First, we noticed that we cannot set the constraint on wellhead pressure. In reality, the wells exhibit fluctuating behaviour only if the well is in operation and connected to a pipe with an operating pressure of 7 bars. If the well is put on silencer (pressure is atmospheric) or shut in, it does not fluctuate. This means that the outlet pressure could trigger the fluctuations and is a crucial condition to be set in the model. However, in our model, the wellhead pressure constraint had to be set atmospheric, otherwise the well would not flow by itself.

Furthermore, the flow rate in well NG-07 was on average 11.7 kg/s and when we converted it to $m^3$/day using pressure and enthalpy values, we obtained a value of 18 433 $m^3$/day. Once again, in our model we could not constrain this value, so we had to modify BHP and constrain the injectors instead. We did not manage to make the well operate exactly at this value, but it operated at a flow rate of around 60 000 $m^3$/day which is three times higher.

Following that, we started experimenting with the time steps and ran a simulation where 1st May - 6th May the flow rate was calculated every hour, from 6th - 10th May once a day and 10th - 11th every 5 minutes. After 11th the time step was set again once a day until the end of the simulation. The result can be seen below in Figure 5.20.

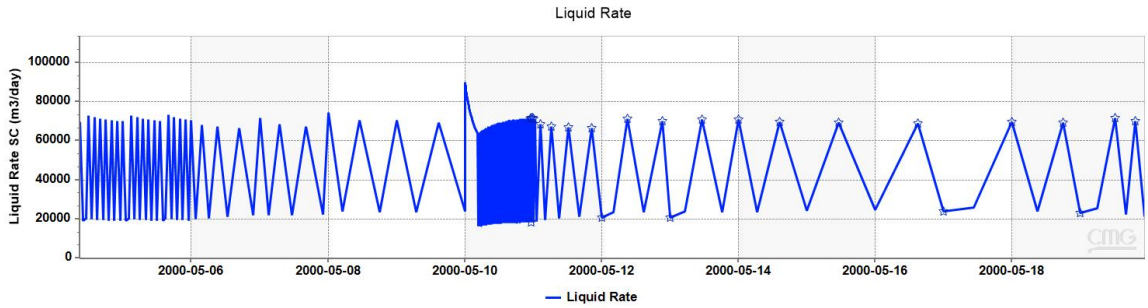


**Figure 5.20:** Flow rate dependency on time steps

This figure shows that the fluctuations in flow rate absolutely depend on the chosen time step. To be more precise, if the time step is set to 1 day, then the liquid rate peaks also occur once a day, and if the time step is set to 1h, the flow rate fluctuates 24 times per day. This oscillation frequency is increased once again in the same pattern when the sampling time step is set to 5 minutes. Naturally, the fluctuations should not be dependent on the chosen time step, and we therefore conclude that these fluctuations are not real and only occur because of numerical errors. The star symbols on top of the peaks indicate a warning saying "Iteration for reference layer pressure fails to converge. Setting ref layer pressure to bottom hole pressure." This error explains that pressure is also artificially lowered, after a peak occurs to comply with the boundary conditions. This error was obtained for all time steps from the time the osculations started in the liquid rate.

Furthermore, it appears that STARS is not equipped to model flow inside the well bore. When visualising 3D plots of water saturation (Figure 5.21) and comparing them to the profiles reported in the software, it seems that the inside of the well correspond to the values in the cell where the well is located. The cell size being 60 m x 60 m x 10 m and our well has a diameter of 0.178 m, we do not believe an accurate modelling of flow in the well is possible. This idea is also supported by the fact that the pressure values in the well did not change when changing the well's inner diameter from 0.4 m to 0.1 m.

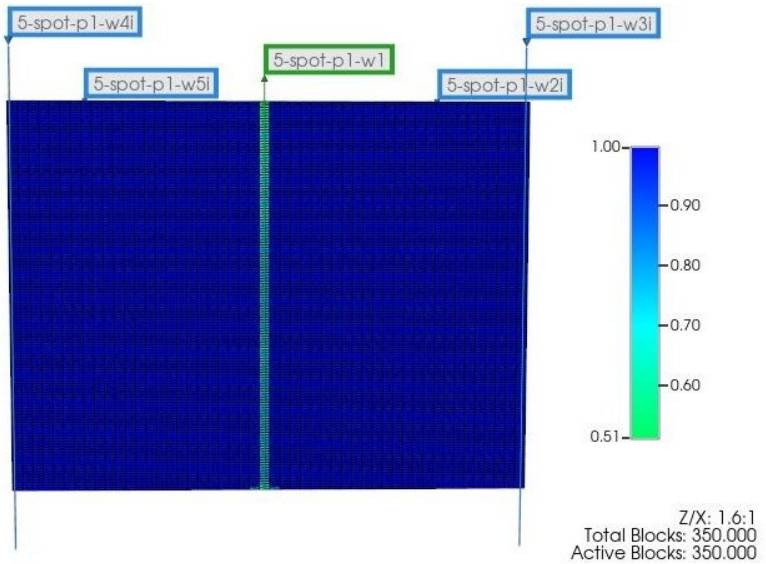


**Figure 5.21:** 3D visualisation of water saturation

## 5.4. Multiple feed zones model from Matsumoto et al. (2020)

The results of the CMG STARS model show that there is two-phase flow present in the well and that it occurs beneath the feed zones, where one phase water flows in. However, the plotted pressure and flow rate fluctuations are likely caused by numerical errors and are therefore not representative. Therefore, the Matsumoto, Itoi, and Fujimitsu [29] model is used to confirm whether interaction between multiple feed zones of different enthalpies is the cause for the fluctuations in wellhead pressure in the Icelandic wells.

An explanation of the model can be found in section 5.4.1, the results were reported in section 5.4.2 and a sensitivity analysis was performed in section 5.4.3.

### 5.4.1. Model

This model uses finite difference methods to solve discretised versions of the conservation of Mass, Energy, and Momentum Equations in the well bore.

$$\partial_t \rho \cdot A + \partial_z(\rho u A) = q_M \tag{5.1}$$

$$\partial_t u + u\,\partial_z u = -\frac{1}{\rho}\,\partial_z P - \frac{1}{2}(K_f + K_d)\,u\,|u| + g\cos\theta \tag{5.2}$$

$$\partial_t(\rho h) \cdot A + \partial_z(\rho h u A) = \partial_t P \cdot A + q_H \tag{5.3}$$

with $P$ the pressure, $\rho$ the density, $u$ the mean velocity, $h$ the mean specific enthalpy, $t$ the time, $z$ the depth, $K_f$ the coefficient due to the pressure loss resulting from the friction between the pipe and the fluid, $q_M$ the mass flow rate, $q_H$ the enthalpy flow rate, $\theta$ the angle of the well, $A$ the cross sectional area of the well and $K_d$ the coefficient of pressure loss due to the diameter changes of the well bore.

To calculate the mass flow rate $q_M$ between the feed zones and the well, Matsumoto et al. (2020) [29] use a simple reservoir model, assuming a well of known diameter, intersecting with two circular reservoirs of known thickness and depths. These reservoir models have constant values for reservoir pressure $P_{re}$ which are used as a boundary condition at the external boundary of the reservoir discs. The reservoir discs also use a constant mean specific enthalpy $h_{re}$, kinematic viscosity $\nu_{re}$, radius $r_e$, permeability $k$, and thickness $w$. This reservoir model distinguishes between three flow regimes: single-phase flow, a transition phase between single- and two-phase flow, and full two-phase flow. The transition phase occurs when the reservoir and feed zone pressures are close to the boiling-point pressure. In this condition, part of the system still behaves as a single-phase flow, while other parts exhibit a two-phase behaviour, creating in a mixture of both flow types [29].

$$q_H = \begin{cases} h_{re}\, q_M, & q_M \geq 0, \\ h\, q_M, & q_M < 0, \quad h = h_{fz} \text{ or } h = h_{re}, \end{cases} \tag{5.4}$$

The flow direction in the feed zones can change direction throughout the simulation, which means that the fluid can flow back to the reservoir at certain times of the cycle. Depending on the assumption made about the specific enthalpy of the fluid flowing from the well bore back to the reservoir, the enthalpy of

the whole system can decrease when it is assumed to be constant. In equation 5.4, a negative flow rate $q_M$ indicates flow towards the reservoir.

In this study the enthalpy of the fluid flowing from the well to the reservoir is assumed to be equal to the enthalpy of the fluid flowing from the reservoir to the well ($h = h_{re}$). Although this is not consistent with energy conservation within the well bore, it maintains overall constant enthalpy throughout the entire system.

If the enthalpy of the fluid leaving the well was equal to $h = h_{fz}$ and $h = h_{re}$ when entering the well, the system would lose enthalpy at a rate of $(h_{fz} - h_{re})q_M$ [29]. This formulation was used by Yamamura et al. [48] and resulted in a dampening in the fluctuation which eventually stopped. Using assumption $h = h_{re}$, Matsumoto, Itoi, and Fujimitsu [29] obtained continuous fluctuations in flow rate and wellhead pressure in time without this dampening effect. The strict conservation of enthalpy at the system scale (well and reservoir) is critical to modelling flow rate instability in geothermal wells. This assumption could be one of the reasons encountered for the difficulty in modelling unstable flow rates using larger, numerical models, such as CMG STARS for example (Matsumoto, 2025, personal communications).

The following parameters were used to model the well behaviour used by M. Matsumoto in his simulator. The value for the enthalpy of the shallow feed zone was chosen based on the 3 most recent temperature measurements. The average is 265 °C which corresponds to enthalpy value of 1160 kJ/kg. 10 °C above and below the average value were used in the Sensitivity analysis. All of the parameters were based on well NG-07, either from technical reports, SCADA or TFT data.

| | |
|---|---|
| Wellbore Inner Diameter | 0.178 m |
| Shallow feed zone depth | 1530 m |
| Deep feed zone depth | 1990 m |
| Shallow feed zone enthalpy | [1100, 1160, 1208] kJ/kg |
| Shallow feed zone temperature | [255, 265, 275] °C |
| Deep feed zone enthalpy | 1493.4 kJ/kg |
| Shallow permeability thickness | $6 \cdot 10^{-13} m^3$ |
| Deep permeability thickness | $1 \cdot 10^{-13} m^3$ |
| Shallow feed zone initial pressure | 11.8 MPa |
| Deep feed zone initial pressure | 14.5 MPa |
| Wellhead pressure | 2.205 MPa |

**Table 5.1:** Model Parameters

### 5.4.2. Simulation results using Matsumoto's model

The results of the simulation, which represent well NG-07, are reported in Figure 5.22. After 4 hours, the model started simulating periodic behaviour. This shows that under the conditions imposed for this simulation, the instability in the well is triggered by the interaction between the feed zones.

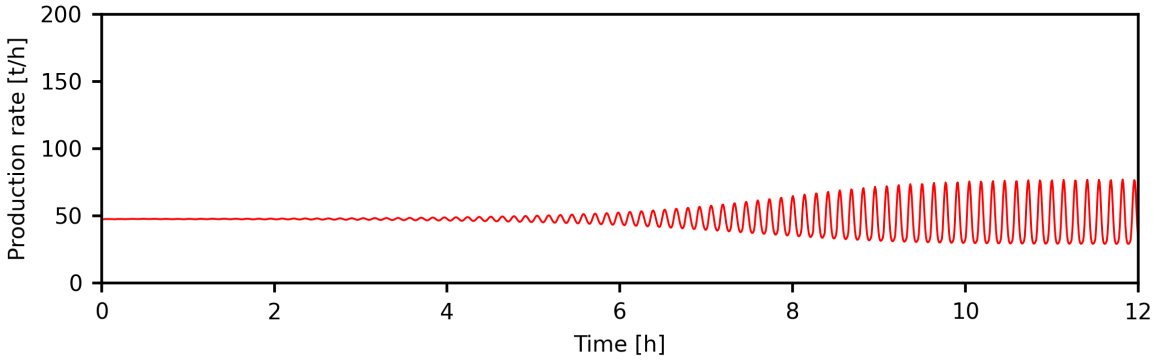


**Figure 5.22:** Fluctuating flow rate with shallow feed zone enthalpy 1160 kJ/kg

Here, the fluctuating behaviour is shown. The period between the peaks is around 9 minutes, which is a lot shorter than in well NG-07 where the fluctuations occur every 6-9 days. However, the flow rate is quite similar: 13.2 kg/s in the simulation compared to 11.7 kg/s in the real well.

### 5.4.3. Sensitivity analysis

A sensitivity analysis was performed by decreasing and increasing the temperature in the shallow feed zone by 10 °C. All other simulation parameters remained identical. This enthalpy change greatly impacts the fluctuations in the well. As can be seen in Figure 5.23, when the temperature is reduced to 255°C , the model exhibits unstable behaviour in the beginning of the simulation and becomes periodic after 6 hours. The larger the enthalpy difference between the shallow and deep feed zone, the slower the well fluctuates. In addition, the amplitude of fluctuations increases, but the average production rate decreases when the shallow feed zone temperature is reduced. Most importantly, the fluctuations come to a complete stop when the shallow feed zone temperature is set to 275 °C.

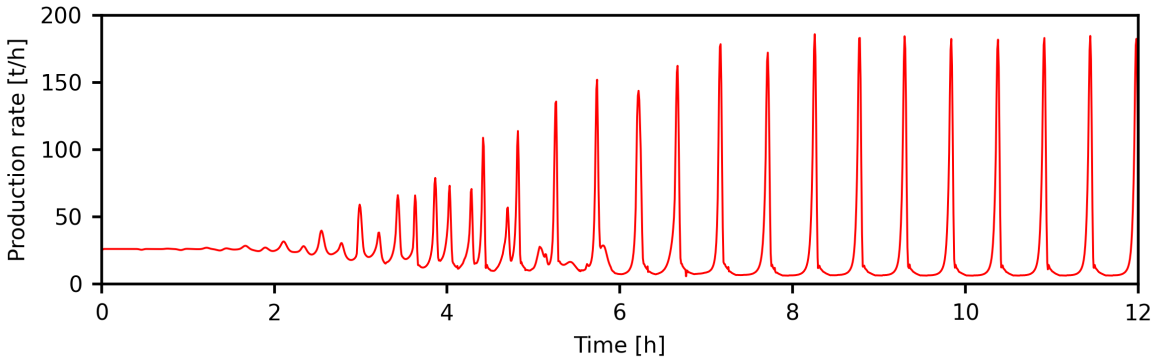


**Figure 5.23:** Fluctuating flow rate with shallow feed zone enthalpy 1100 kJ/kg

In Figure 5.23 it can be seen that the average production rate throughout the simulation was 7.22 kg/s, being less than the flow rate from well NG-07, 11.7 kg/s. Additionally, the simulated production rate peaks occur every half an hour while well NG-07 has a fluctuating period of 6-9 days. This means that the decreased enthalpy of the shallow feed zone results in a more realistic flow rate frequency, but a less accurate flow rate than in well NG-07.

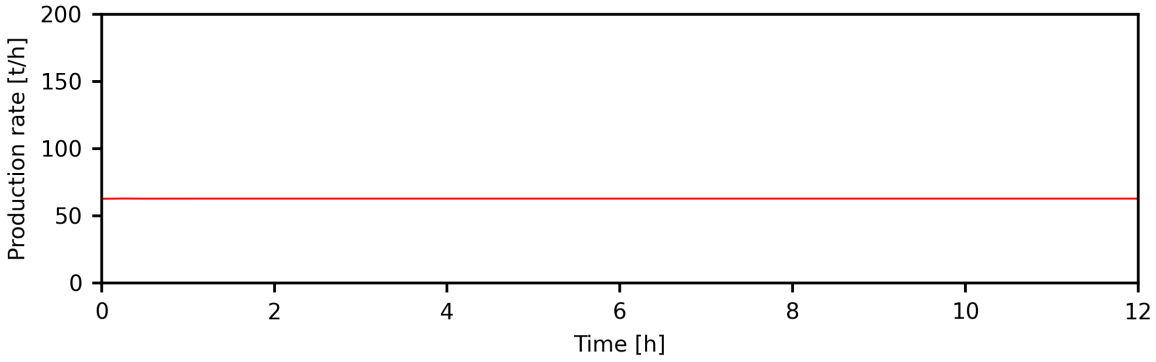


**Figure 5.24:** Flow rate with shallow feed zone enthalpy 1208 kJ/kg

Figure 5.24 shows that the fluctuating behaviour disappears when the temperature of the shallow feed zone reaches 275°C. This highlights the importance of the difference in enthalpy between the two feed zones to obtain a fluctuation in the production rate. To confirm whether pressure fluctuations in the Icelandic wells originate from the interaction between multiple feed zones of different enthalpy, accurate enthalpy measurements along the wellsa, especially at the feed zones, must be conducted, as a slight change of only 10 °C in the temperature of the shallow feed zone has a significant impact on the simulation results.

### 5.4.4. Limitations

As mentioned in Section 5.2, this simulation was performed using a homogeneous flow model with no-slip between the water and the gas phase. The flow velocity of the gas and vapour phase inside the well are then assumed to be equal. According to Matsumoto (2025, personal communications), if a slip model is used, periodic flow can be generated with higher shallow feed zone temperatures than in the homogeneous flow model. However, the slip model results in periodic flow only in a very narrow temperature range. Consequently, our Multiple feed zone theory can be further tested using the slip model to assess if the fluctuations also appear in this case.

The model used by Matsumoto et al. (2020) [29] only takes into account two feed zones. However, as can be seen in Figure 2.10, well NG-07 is recharged by many more feed zones of different sizes. Using a similar model that would encompass more than two feed zones would then confirm if fluctuations can occur in wells that feature not only two main feed zones, but more and of various sizes.

Furthermore, this model uses the wellhead pressure as a boundary condition; therefore, it is constant in time throughout the simulation. However, well NG-07 does not feature a constant wellhead pressure, and the effect of variations in flow rate on the top hole pressure should be considered. This was done by Matsumoto, Itoi, and Fujimitsu [29] by extending the well bore model by 2000 metres from the wellhead as seen in Figure 5.6, and the results can be seen in Figure **??**. Due to time constraints, this extended model could not be used.

# 6 Discussion

The models introduced aim to capture different phenomena. One is based on fluid dynamics and the other is based on thermodynamics. However, the consequent outcome for both models - STARS and the 1D well bore numerical model, is simulating the offset conditions for the observed two phase flow instability.

## 6.1. Internal Flow Instability

Now, let us evaluate the quality of results from § 4.3.2, outlining the limitations and assumptions in the developed 1D numerical model.

Firstly, we assumed the enthalpy to be constant along the whole well. For future research, we recommend a more detailed enthalpy profile, be it a (e.g. linear) interpolation between top and bottom hole enthalpy or an empirical profile based on along hole observations. The implications of this simplification may have given an underestimation of internal pressure drop, since the fluid along the well is in reality hotter than in the model.

Moreover, this model does not account for the perforations and multiple inflow zones along the pipe, but instead simulates a solid casing until 2000 m depth. A more detailed model can be built by stacking multiple feed zones, as described in Ch. 6.9 of Jansen [23]. This more complex model could even be used to further validate the Multiple Feed Zone hypothesis.

A comparison with real data shows that our model is not able to capture the operational conditions. The $\dot{m}$ and $WHP$ presented in Table 4.1 are not a solution of the Tubing Performance Curve (Figure 4.19).

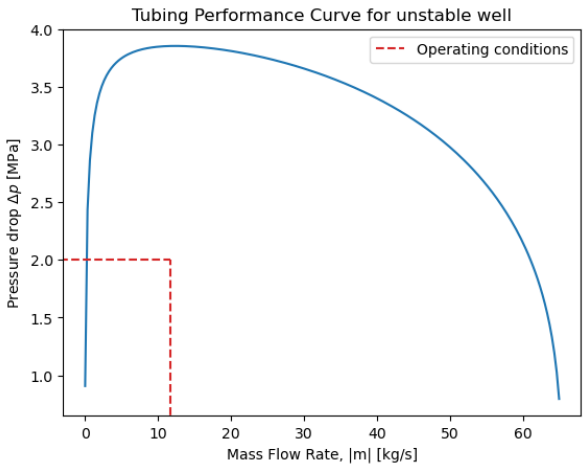


**Figure 6.1:** Tubing Performance with Operating Conditions

Overall, it is worth following research in this topic. A better model (HOLA, WELL-3, WELL-4, etc.) could be used to improve and validate these results. Some of these softwares are time sensitive, and may be able to simulate the amplitude and frequency of the fluctuations.

As mentioned previously, changes in individual phase flow velocities are the main driver for cyclic flow pattern transitions. Therefore, a mitigation measure for liquid hold-up and pressure drop oscillations is to artificially increase the overall flow rate. This could be achieved by artificially reducing the inner diameter of the well, since smaller diameters increase the frictional pressure drop, which can stabilise the flow regime and prevent liquid hold-up [8]. A common mitigation approach is to employ a pipe of smaller diameter in the production zone of the well or, as a less cost intensive temporary solution, to run down a velocity string within the existing piping [49]. The velocity string effectively decreases the diameter of the well and consequently increases the overall flow rate which supports liquid unloading in the well [49, 33]. The effect of the choice of a smaller radius in our developed model is shown in figure 6.2. According to our simulation, the operating point is further shifted to the right branch of the curve, suggesting more stable operating conditions.

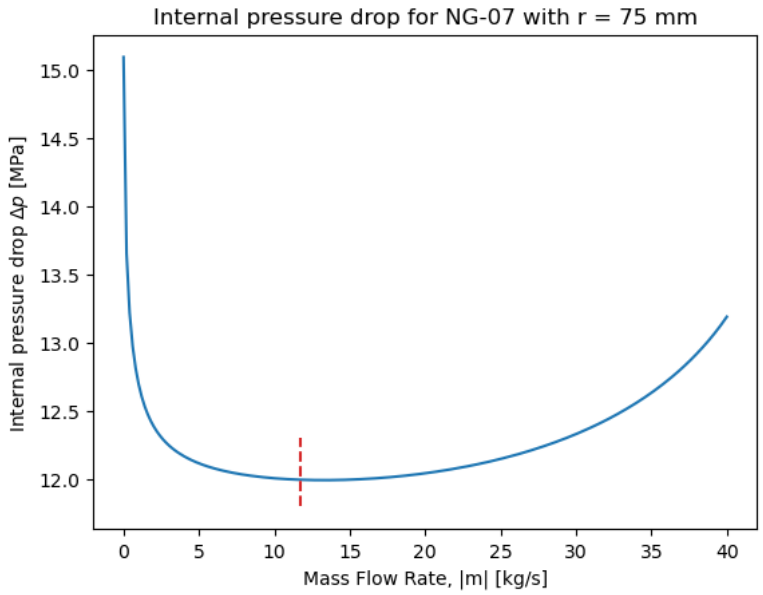


**Figure 6.2:** Effect of reduction of the inner radius to r = 75 mm on the operating point of well (NG-07).

Furthermore, Hu and Golan also showed that the addition of throttling (e.g., choke) at the wellhead can stabilise gas- or steam-lifted systems by damping pressure oscillations [20].

## 6.2. Multiple Feed Zones

The Multiple Feed Zone theory was supported by modelling water saturation down the well in STARS and replicating flow rate fluctuations using Matsumoto's analytical model. Results from STARS show that we have two phase flow in the well and the graphs prove that the critical condition of two phase flow being trapped underneath a single phase flow for Multiple Feed Zone theory is met.

However, we are unsure if CMG STARS model is equipped for accurate modelling of flow inside a well bore, because:

- It was not possible to set the desired constraints on the wellhead pressure and flow rate to replicate well NG-07 exactly. That is why, in the results, flow rate and frequency are both significantly higher than in well NG-07.

- Changing the well bore diameter from 0.1 m to 0.4 m did not change the pressure or flow rate values.

Furthermore, fluctuations in flow rate were replicated but could be caused by numerical errors. This is suspected because of the warning messages and the frequency being dependent on the chosen time step. Therefore, we are not relying on the pressure and flow rate outcomes from STARS, but trust only the water saturation profiles. Even though the STARS outcomes did not reliably prove fluctuations in the flow rate, Matsumoto's model did. The results of his model showed fluctuations in the flow rate using parameters taken from well NG-07. We did not have continuous flow rate measurements to compare these replicated values directly. However, we could compare the frequencies of flow rate and well head pressure, because they have the same period [29]. We found that the simulated fluctuations have a period of 9 minutes, while in NG-07 it is 6-9 days. Additionally, his model uses homogeneous flow which does not imitate reality very precisely.

## 6.3. Future Research

In future research the FlexWell feature in STARS or other well bore modelling software should be used to validate the results. Furthermore, Matsumoto's new model that accounts for slip could be tested with our parameters to validate whether fluctuations also occur in more realistic scenarios. The model including slip should be able to model fluctuations in situations with higher enthalpies, but has a relatively narrow shallow feed zone temperature range where the flow becomes periodic (Matsumoto and Yoshida [30], personal communication).

For the Internal Flow Instability hypothesis, the model could be adjusted to simulate two-phase flow instability in a system with more than one feed zone. Due to time constraints, this option was not explored further within this project, but would be a considerable addition for further research. This could also provide an opportunity to compare the results of this model to the ones we obtained from the STARS model and the approach of Matsumoto, as pressure and flow conditions, as well as the void fraction and water content, can be derived at the additional nodes introduced.

Furthermore, having more accurate data would also increase the accuracy of the models. The temperature values at feed zones were interpolated from measurements taken every 100 m which represents a very coarse resolution and contributes to the uncertainty. Additionally, permeability and porosity values had to be assumed or taken from the relevant literature. However, these could be very different in reality.

# 7 Conclusion

This study aims to find an explanation for the pressure fluctuations present at the wellhead of five high enthalpy geothermal wells in the Hellisheiði and Nesjavellir geothermal fields. Two different hypotheses were investigated to answer this research question.

The results from the Internal Flow Instability hypothesis indicate that Ledinegg instability could occur in the wells. However they don't give indications as to why the system remains in the unstable condition, and does not shift to a more stable solution.

As for the Multiple Feed Zone hypothesis, the STARS model shows that the required two phase conditions can be achieved, and fluctuations can be replicated in the model by Matsumoto.

Comparing both hypotheses, the authors would like to outline that there is more solid evidence for the Multiple Feed Zones hypothesis, and that it could be more easily tested by improving the pressure and temperature data accuracy along the well.

Future research guidelines include improving the quality of the data -especially the along hole pressure and temperature distribution ideally while the well is in operation; together with an energy component for the Internal Flow Instability model, and the use of FlexWell in STARS.

# 8 Appendix A

| | |
|---|---|
| Wellbore depth | 2000 m |
| Wellbore length | 2000 m |
| Casing length | 600 m |
| Inner tubing | 0.089 m |
| Outer tubing | 0.0968 m |
| Insulation | 0.1 m |
| Inner casing | 0.1 m |
| Outer casing | 0.122 m |
| Hole | 0.14 m |

**Table 8.1:** Wellbore model used in STARS

| | |
|---|---|
| Wellbore depth | 2000 m |
| Wellbore length | 2000 m |
| Casing length | 600 m |
| Inner tubing | 0.1 m |
| Outer tubing | 0.114 m |
| Insulation | 0.309 m |
| Inner casing | 0.309 m |
| Outer casing | 0.340 m |
| Hole | 0.445 m |

**Table 8.2:** Largest wellbore model used in STARS

| | |
|---|---|
| Wellbore depth | 2000 m |
| Wellbore length | 2000 m |
| Casing length | 600 m |
| Inner tubing | 0.062 m |
| Outer tubing | 0.073 m |
| Insulation | 0.119 m |
| Inner casing | 0.119 m |
| Outer casing | 0.140 m |
| Hole | 0.200 m |

**Table 8.3:** Smallest wellbore model used in STARS

# 9 Appendix B

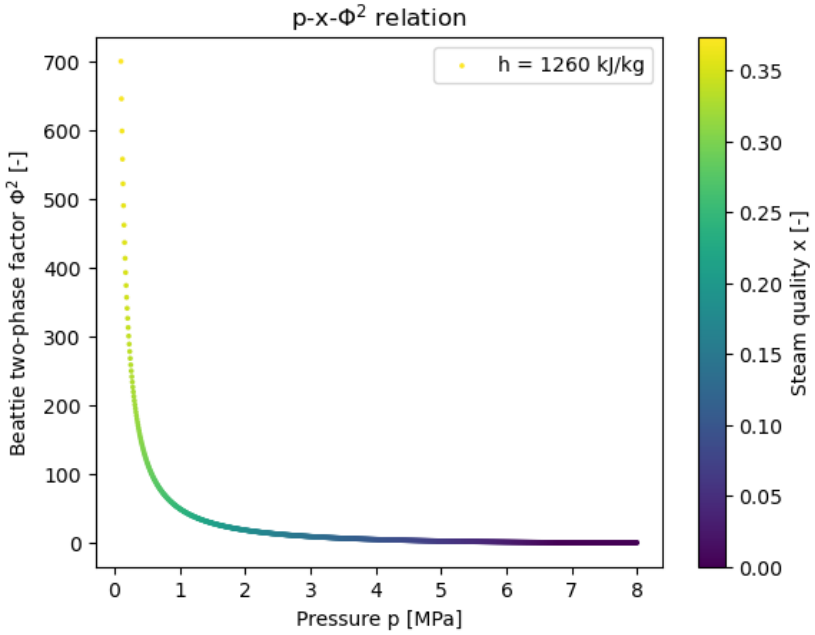


**Figure 9.1:** Beattie (1973) correlation between pressure, steam fraction and void fraction for constant h=1260 kJ/kg

# References


[1] Naief Almalki and Wael H. Ahmed. "Evaluating the two-phase flow development through orifices using a synchronised multi-channel void fraction sensor". In: *Experimental Thermal and Fluid Science* 118 (2020), p. 110165. DOI: https://doi.org/10.1016/j.expthermflusci.2020.110165.

[2] Maziad Alsanea, Camilo Mateus-Rubiano, and Hamidreza Karami. "Liquid loading in natural gas vertical wells: A review and experimental study". In: *SPE Production & Operations* 37.3 (2022), pp. 554–571. DOI: 10.2118/209819-PA. URL: https://doi.org/10.2118/209819-PA.

[3] D. Barnea. "Transition from annular flow and from dispersed bubble flow—unified models for the whole range of pipe inclinations". In: *International Journal of Multiphase Flow* 12.5 (1986), pp. 733–744. ISSN: 0301-9322. DOI: https://doi.org/10.1016/0301-9322(86)90048-0. URL: https://www.sciencedirect.com/science/article/pii/0301932286900480.

[4] D.R.H. Beattie. "A note on the calculation of two-phase pressure losses". In: *Nuclear Engineering and Design* 25.3 (1973), pp. 395–402.

[5] Grimur Bjornsson et al. "Development of a 3-D geothermal reservoir model for the greater Hengill volcano in SW-Iceland". In: TOUGH Symposium, 2003. URL: https://tough.lbl.gov/assets/files/02/documentation/proceedings/2003-BjornssonHiartarsonBo.pdf.

[6] G. Bodvarsson et al. "A summary of modeling studies of the Nesjavellir geothermal field, Iceland". In: (Jan. 1988).

[7] N P Cheremisinoff and R Gupta. *Handbook of fluids in motion*. Butterworth Publishers,Woburn, MA, USA, Dec. 1982. URL: https://www.osti.gov/biblio/6214053.

[8] H. Duns and N. C. J. Ros. "Vertical flow of gas and liquid mixtures in wells". In: *Proceedings of the 6th World Petroleum Congress*. 6th World Petroleum Congress (Frankfurt am Main, Germany). Section II, Paper 22–PD 6. World Petroleum Congress. 1963, pp. 451–465.

[9] H Franzson and H Sigvaldason. *NESJAVELLIR, HOLA NG-7: Jarðlög, ummyndun, mælingar og vatnsædar*. Tech. rep. 05-85124/ JHD-18. Dec. 1985.

[10] Government of Iceland. *Geothermal*. https://www.government.is/topics/business-and-industry/energy/geothermal/. Retrieved October 29, 2025, from the Government of Iceland website. n.d.

[11] H. Guðmundsdóttir. "A Coupled Wellbore-Reservoir Simulator utilizing Measured Wellhead Conditions". In: (2012). Faculty of Mechanical Engineering, University of Iceland.

[12] Á Guðmundsson et al. *NESJAVELLIR Hola NJ-20. 3. Áfangi: Borun vinnsluhluta í 1800 m dýpi*. Tech. rep. OS-99069. Sept. 1999.

[13] Á Guðmundsson et al. *Nesjavellir, hola NJ-20: 2. afangi: Borun fyrir 9 5/8" vinnslufóðringu i 773 m dypi*. Tech. rep. OS-OS-99030. Apr. 1998.

[14] Gunnar Gunnarsson and Edda S. P. Aradóttir. "The Deep Roots of Geothermal Systems in Volcanic Areas: Boundary Conditions and Heat Sources in Reservoir Modeling". In: *Transport in Porous Media* 108.1 (May 2015). DOI: 10.1007/s11242-014-0328-1. URL: https://doi.org/10.1007/s11242-014-0328-15.

[15] B.S. Hardarson et al. “Volcano-Tectonic-Geothermal Interaction at the Hengill Triple Junction, SW Iceland”. In: *GRC Transactions* 33 (2009). URL: https://publications.mygeoenergynow.org/grc/1028427.pdf.

[16] A. R. Hasan, C. S. Kabir, and C. Sarica. *Fluid Flow and Heat Transfer in Wellbores*. USA: Society of Petroleum Engineers, 2002.

[17] Sarah Helbig and Sadiq J. Zarrouk. “Measuring two-phase flow in geothermal pipelines using sharp edge orifice plates”. In: *Geothermics* 44 (2012), pp. 52–64. DOI: https://doi.org/10.1016/j.geothermics.2012.07.003. URL: https://www.sciencedirect.com/science/article/pii/S0375650512000405.

[18] H. M. Helgadóttir et al. *Hellisheiði – Hola HE-59: Forborun, 1., 2. og 3. áfangi: Borun fyrir yfirborðsfóðringu í 115 m, öryggisfóðringu í 317 m, vinnslufóðringu í 800 m og götuðum leiðara í 1130 m dýpi Dýpi holu er 2381 m*. Tech. rep. ÍSOR-2016/046. Oct. 2015.

[19] Geoffrey F. Hewitt and George Yadigaroglu. “Modelling Strategies and Two-Phase Flow Models”. In: *Introduction to Multiphase Flow: Basic Concepts, Applications and Modelling*. Ed. by George Yadigaroglu and Geoffrey F. Hewitt. Cham: Springer International Publishing, 2018, pp. 39–77. ISBN: 978-3-319-58718-9. DOI: 10.1007/978-3-319-58718-9_2. URL: https://doi.org/10.1007/978-3-319-58718-9_2.

[20] Bin Hu and Michael Golan. “Gas-lift instability resulted production loss and its remedy by feedback control: Dynamical simulation results available”. In: SPE International Improved Oil Recovery Conference in Asia Pacific (Kuala Lumpur, Malaysia, Oct. 2003). SPE Paper 84917-MS, presented October 20, 2003. Society of Petroleum Engineers (SPE). 2003. DOI: 10.2118/84917-MS. URL: https://doi.org/10.2118/84917-MS.

[21] Shaul Hurwitz and Michael Manga. “The Fascinating and Complex Dynamics of Geyser Eruptions”. In: *Annual Review of Earth and Planetary Sciences* 45.1 (Apr. 2017), pp. 31–59. DOI: 10.1146/annurev-earth-063016-015605. URL: https://doi.org/10.1146/annurev-earth-063016-015605.

[22] S. E. Ingebritsen and S. A. Rojstaczer. “Controls on Geyser Periodicity”. In: *Science* 262.5135 (Nov. 1993), pp. 889–892. DOI: 10.1126/science.262.5135.889. URL: https://doi.org/10.1126/science.262.5135.889.

[23] J.D. Jansen. *Nodal Analysis of Oil and Gas Production Systems*. 1th ed. Society of Petroleum Engineers, 2017.

[24] Tamie Jovanelly. *Iceland : Tectonics, Volcanics, and Glacial Features*. 1st ed. American Geophysical Union, 2020.

[25] Mb Ledinegg. “Instability of flow during natural and forced circulation”. In: *Die Wärme* 61 (1938).

[26] Xinli Lu et al. “Experimental investigation and numerical modelling of transient two-phase flow in a geysering geothermal well”. In: *Geothermics* 35.4 (Aug. 2006), pp. 409–427. DOI: 10.1016/j.geothermics.2006.07.001. URL: https://doi.org/10.1016/j.geothermics.2006.07.001.

[27] Matteo Lupi et al. “Geysers, Boiling Groundwater and Tectonics: The 3D Subsurface Resistive Structure of the Haukadalur Hydrothermal Field, Iceland”. In: *Journal of Geophysical Research Solid Earth* 127.11 (Oct. 2022). DOI: 10.1029/2022jb024040. URL: https://doi.org/10.1029/2022jb024040.

[28] *map.is*. URL: https://www.map.is/os/.

[29] Mitsuo Matsumoto, Ryuichi Itoi, and Yasuhiro Fujimitsu. “Theoretical study of conditions for generation of periodic wellbore flow due to inflow of a lower-enthalpy fluid”. In: *Geothermics* 89

(Sept. 2020), p. 101948. DOI: 10.1016/j.geothermics.2020.101948. URL: https://doi.org/10.1016/j.geothermics.2020.101948.

[30] Mitsuo Matsumoto and Naoto Yoshida. "Theoretical Study of Conditions for Generation of Periodic Wellbore Flow: Dependence on Two-Phase Flow Models". In: *47th New Zealand Geothermal Workshop* (Nov. 2025). ISSN: 2703-4275.

[31] Saeid Mokhatab and William A. Poe. "Chapter 3 - Raw Gas Transmission". In: *Handbook of Natural Gas Transmission and Processing (Second Edition)*. Ed. by Saeid Mokhatab and William A. Poe. Second Edition. Boston: Gulf Professional Publishing, 2012, pp. 85–180. ISBN: 978-0-12-386914-2. DOI: https://doi.org/10.1016/B978-0-12-386914-2.00003-0. URL: https://www.sciencedirect.com/science/article/pii/B9780123869142000030.

[32] J. O'Sullivan. *Introduction to geothermal science and engineering*. Engineering Science, University of Auckland, New Zealand. [PDF]. n.d. URL: https://www.irena.org/-/media/Files/IRENA/Agency/Events/2014/Jun/2/1_Sullivan.pdf?la=en&hash=7B8C0F4B0F52944710B21166BFC30352DD7AC288.

[33] Pieter Oudeman. "On the flow performance of velocity strings to unload wet gas wells". In: *SPE Middle East Oil and Gas Show and Conference*. SPE. 2007, SPE–104605.

[34] S. Ragnarsson. *ISE Energy field school*. [Presentation slides; PowerPoint]. Aug. 2024.

[35] Sigurður Ragnarsson. *Production Fields of Hellisheiði and Nesjavellir Power Plants: Past, Present and Future*. Paper presented at the JFÍ Spring Conference, March 14, 2025. Mar. 2025.

[36] Ayush Rastogi and Yilin Fan. "Experimental investigation and modeling of onset of liquid accumulation in large-diameter deviated gas wells". In: *Journal of Natural Gas Science and Engineering* (2019). SPE Paper 196130-MS. DOI: 10.2118/196130-MS. URL: https://doi.org/10.2118/196130-MS.

[37] Thomas M. P. Ratouis et al. "Modelling the Complex Structural Features Controlling Fluid Flow at the CarbFix2 Reinjection Site, Hellisheiði Geothermal Power Plant, SW-Iceland". In: *44th Workshop on Geothermal Reservoir Engineering* (2019).

[38] S.Z. Rouhani and E. Axelsson. "Calculation of void volume fraction in the sub cooled and quality boiling regions". In: *International Journal of Heat and Mass Transfer* 13 (1970), pp. 383–393.

[39] Maxwell L. Rudolph and Robert A. Sohn. "A model for internal oscillations in geysers, with application to Old Faithful (Yellowstone, USA)". In: *Journal of Volcanology and Geothermal Research* 343 (May 2017), pp. 17–24. DOI: 10.1016/j.jvolgeores.2017.04.023. URL: https://doi.org/10.1016/j.jvolgeores.2017.04.023.

[40] Leonardo Carlos Ruspini, Christian Pablo Marcel, and Alejandro Clausse. "Two-phase flow instabilities: A review". In: *International Journal of Heat and Mass Transfer* 71 (2014), pp. 521–548. ISSN: 0017-9310. DOI: https://doi.org/10.1016/j.ijheatmasstransfer.2013.12.047. URL: https://www.sciencedirect.com/science/article/pii/S0017931013010922.

[41] A.N. Shulyupin. "Steam-water flow instability in geothermal wells". In: *International Journal of Heat and Mass Transfer* 105 (Oct. 2016), pp. 290–295. DOI: 10.1016/j.ijheatmasstransfer.2016.09.092. URL: https://doi.org/10.1016/j.ijheatmasstransfer.2016.09.092.

[42] M. A. Sigurgeirsson et al. *Hellisheiði – Hola HE-62: 3. áfangi: Borun fyrir 95/8" götuðum leiðara í 2260 m dýpi*. Tech. rep. ÍSOR-2018/089. Dec. 2018.

[43] O Sigurosson and E Gunnlaugsson. *NESJAVELLIR: Hola NJ-15, 4.afangi Upphitun, upphleyping, blastur og jofnun prystings eftir blastur*. Tech. rep. OS-88023/JHD-13 B. June 1988.

[44] The Engineering Toolbox. *Surface Roughness Coefficients*. 2003. URL: https://www.engineeringtoolbox.com/surface-roughness-ventilation-ducts-d_209.html.

[45] A. J. Torre et al. "Casing heading in flowing oil wells". In: *SPE Production Engineering* 2.04 (Nov. 1987), pp. 297–304. DOI: 10.2118/13801-pa. URL: https://doi.org/10.2118/13801-pa.

[46] W. Wagner et al. "The IAPWS Industrial Formulation 1997 for the Thermodynamic Properties of Water and Steam". In: *Journal of Engineering for Gas Turbines and Power* 122.1 (Jan. 2000), pp. 150–184. ISSN: 0742-4795. DOI: 10.1115/1.483186. eprint: https://asmedigitalcollection.asme.org/gasturbinespower/article-pdf/122/1/150/5548474/150_1.pdf. URL: https://doi.org/10.1115/1.483186.

[47] Sin-Mei Wu et al. "Imaging the Subsurface Plumbing Complex of Steamboat Geyser and Cistern Spring With Hydrothermal Tremor Migration Using Seismic Interferometry". In: *Journal of Geophysical Research Solid Earth* 126.4 (Mar. 2021). DOI: 10.1029/2020jb021128. URL: https://doi.org/10.1029/2020jb021128.

[48] Keisuke Yamamura et al. "Numerical Analysis of Transient Steam-Water Two-Phase Flow in Geothermal Production Wells with Multiple Feed Zones". In: Stanford University, Feb. 2017.

[49] Zhongbo Zhai et al. "Investigation of the effectiveness of velocity string to improve gas well productivity". In: *Petroleum Science and Technology* 42.8 (2024), pp. 958–973.